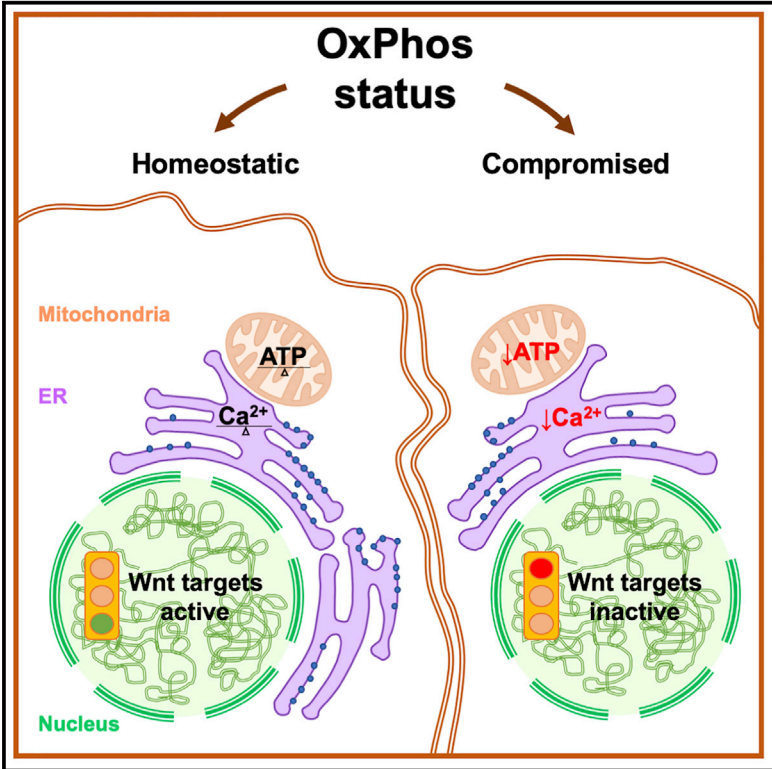# Impaired Mitochondrial ATP Production Downregulates Wnt Signaling via ER Stress Induction

Graphical Abstract

Authors

Roberto Costa, Roberta Peruzzo, Magdalena Bachmann, ..., Sirio Dupont, Ildikò Szabò, Luigi Leanza

Correspondence

ildi@civ.bio.unipd.it (I.S.),
luigi.leanza@unipd.it (L.L.)

In Brief

Wnt signaling and mitochondrial fitness are both important for cell fate. Costa et al. demonstrate that the reduction of mitochondrial ATP production leads to the induction of ER stress and, in turn, decreases canonical Wnt/β-catenin signaling *in vitro* and *in vivo*.

Highlights

- Mitochondrial ATP is necessary to sustain Wnt signaling

- Respiratory chain complex inhibition leads to reduced calcium uptake into the ER

- A defect in complex III assembly causes impairments in Wnt signaling

Impaired Mitochondrial ATP Production Downregulates Wnt Signaling via ER Stress Induction

Roberto Costa,[1,9] Roberta Peruzzo,[1,9] Magdalena Bachmann,[1] Giulia Dalla Montà,[1] Mattia Vicario,[2] Giulia Santinon,[3] Andrea Mattarei,[4] Enrico Moro,[3] Rubén Quintana-Cabrera,[1,5,10] Luca Scorrano,[1,5] Massimo Zeviani,[6,11] Francesca Vallese,[2] Mario Zoratti,[2,7] Cristina Paradisi,[8] Francesco Argenton,[1] Marisa Brini,[1] Tito Calì,[2] Sirio Dupont,[3] Ildikò Szabò,[1,7,*] and Luigi Leanza[1,12,*]

[1]Department of Biology, University of Padova, Padova, Italy
[2]Department of Biomedical Sciences, University of Padova, Padova, Italy
[3]Department of Molecular Medicine, University of Padova, Padova, Italy
[4]Department of Pharmaceutical and Pharmacological Sciences, University of Padova, Padova, Italy
[5]Venetian Institute of Molecular Medicine, Padova, Padova, Italy
[6]MRC Mitochondrial Biology Unit, University of Cambridge, Cambridge, UK
[7]CNR Institute of Neuroscience, Padova, Italy
[8]Department of Chemical Sciences, University of Padova, Padova, Italy
[9]These authors contributed equally
[10]Present address: Consejo Superior de Investigaciones Científicas (CSIC), Institute of Functional Biology and Genomics, University of Salamanca, Salamanca, Spain
[11]Present address: Department of Neurosciences, University of Padova, Padova, Italy
[12]Lead Contact
*Correspondence: ildi@civ.bio.unipd.it (I.S.), luigi.leanza@unipd.it (L.L.)
https://doi.org/10.1016/j.celrep.2019.07.050

SUMMARY

Wnt signaling affects fundamental development pathways and, if aberrantly activated, promotes the development of cancers. Wnt signaling is modulated by different factors, but whether the mitochondrial energetic state affects Wnt signaling is unknown. Here, we show that sublethal concentrations of different compounds that decrease mitochondrial ATP production specifically downregulate Wnt/β-catenin signaling in vitro in colon cancer cells and in vivo in zebrafish reporter lines. Accordingly, fibroblasts from a GRACILE syndrome patient and a generated zebrafish model lead to reduced Wnt signaling. We identify a mitochondria-Wnt signaling axis whereby a decrease in mitochondrial ATP reduces calcium uptake into the endoplasmic reticulum (ER), leading to endoplasmic reticulum stress and to impaired Wnt signaling. In turn, the recovery of the ATP level or the inhibition of endoplasmic reticulum stress restores Wnt activity. These findings reveal a mechanism that links mitochondrial energetic metabolism to the control of the Wnt pathway that may be beneficial against several pathologies.

INTRODUCTION

Mitochondria are central organelles for both cell survival and death. Targeting mitochondrial metabolism to specifically trigger the release of cytochrome c and thus to induce apoptosis in can-

cer cells is emerging as a successful strategy (Fulda et al., 2010). In contrast, how mitochondrial metabolism affects downstream signaling pathways in the context of proliferation and/or differentiation is still poorly defined.

An important signaling pathway affecting cell fate is the canonical Wnt signaling, which relies on the progressive accumulation of unphosphorylated β-catenin in the cytoplasm and its translocation into the nucleus to act as a transcriptional co-activator of a plethora of transcription factors, including the T cell factor-lymphoid enhancer factor (TCF-LEF) family. In the absence of Wnt ligands, β-catenin is degraded by the destruction complex, which includes glycogen synthase kinase 3β (GSK3β) (Morris and Huang, 2016).

Aberrant Wnt/β-catenin signaling is often constitutively activated in cancer cells (e.g., Morris et al., 2010), including breast (Nusse and Varmus, 1982) and colon cancers (Korinek et al., 1997), thereby actively participating in conferring unlimited proliferative potential to these pathologic cells. Small molecules inhibiting Wnt signaling recently entered clinical testing (Zhang and Lum, 2018). Alternatively, activation of Wnt-induced pathways was proposed as a strategy to promote axonal growth after injury (Garcia et al., 2018). While Wnt signaling is well known to influence mitochondrial function (e.g., Bernkopf and Behrens, 2018; Rasmussen et al., 2018; Yoon et al., 2010), the possibility that pharmacological agents affecting mitochondrial metabolism specifically and systematically modulate Wnt signaling has not been explored so far. Here, we show that the fine-tuning of mitochondrial function leads to Wnt signaling modulation both in vitro and in vivo, and we identify the underlying mechanism.

RESULTS

To monitor Wnt signaling in intact cells, human embryonic kidney (HEK293) cells were transiently transfected with a TCF-LEF
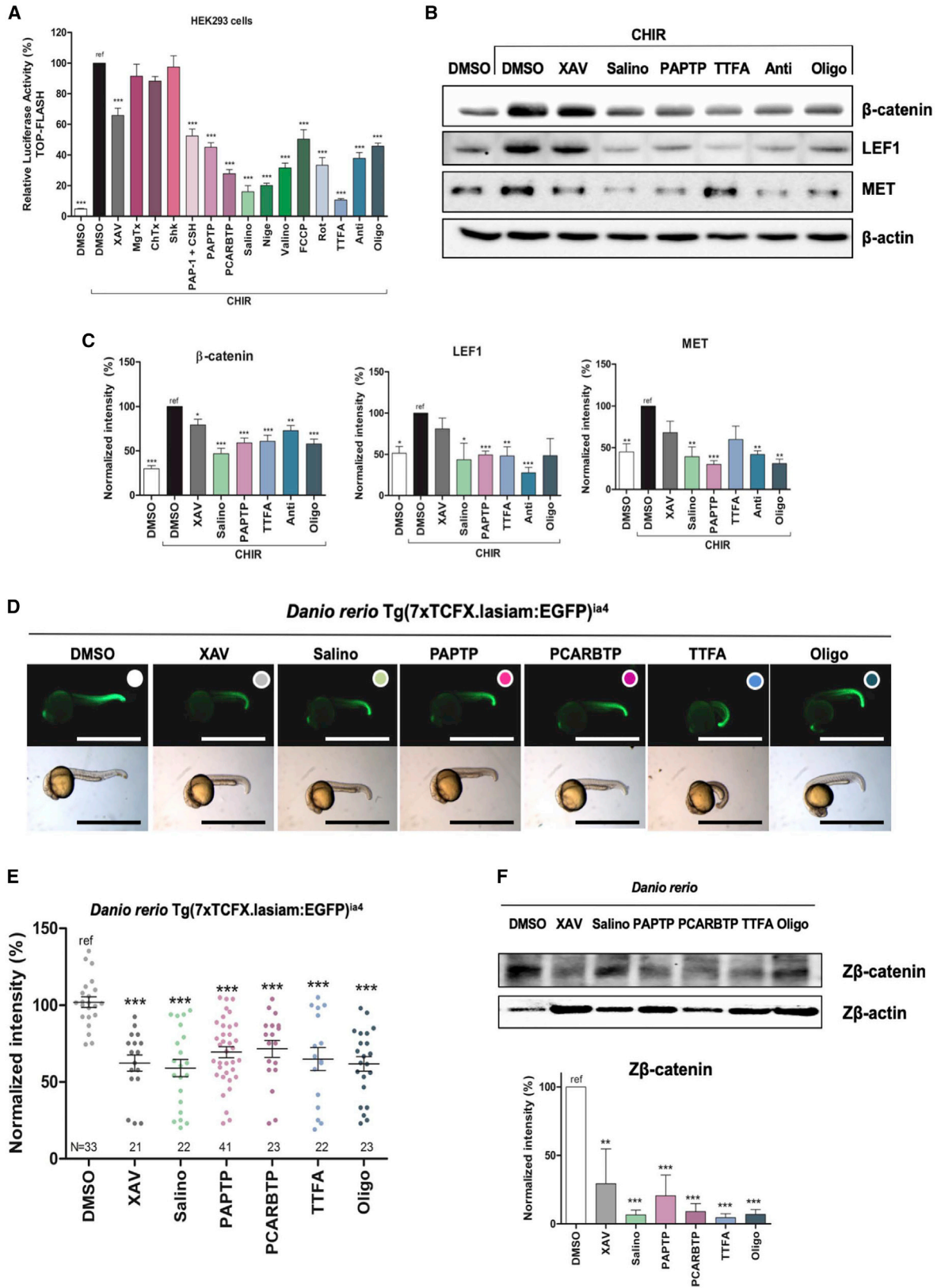
(legend on next page)

luciferase reporter plasmid (Figure 1A). As basal Wnt signaling is relatively low in these cells (Figure S1A), the GSK3 inhibitor CHIR99021 was used to enhance β-catenin stabilization and activate Wnt signaling. The tankyrase inhibitor XAV939, a known Wnt-signaling inhibitor that stabilizes Axin and thus promotes the degradation of cytosolic β-catenin, was used as positive control (Figure 1A) (Shimizu et al., 2012). To test whether the alteration of mitochondrial metabolic stress elicited by different means could alter Wnt signaling, cells were incubated for 8 h with sublethal doses (Figure S1B) of different drugs known to alter mitochondrial function. For our study, we selected a few compounds on the basis of their known effects on respiratory chain complexes or K⁺ fluxes or in their activity as an uncoupler agent (listed below).

The classical uncoupler carbonilcyanide p-trifluoromethoxy-phenylhydrazone (FCCP) and inhibitors of mitochondrial respiratory chain complexes, namely rotenone for complex I, thenoyltrifluoroacetone (TTFA) for complex II, antimycin A for complex III, and oligomycin for complex V, were used (Figure 1A). Similar concentration ranges were directly shown to inhibit complex I, II, III, and V activities in HEK293 cells (e.g., Chrétien et al., 2018), without being toxic at the dosage used (Chrétien et al., 2018; Figures S1B and S1C). According to a vast amount of data from the literature, these compounds markedly alter bioenergetic efficiency in mitochondria (including oxygen consumption rate, ATP production, and reactive oxygen species [ROS] release) (Nicholls, 2013).

Since mitochondrial potassium fluxes also affect the membrane potential across the inner mitochondrial membrane and, as a consequence, trigger the release of ROS (Laskowski et al., 2016; Szabo and Zoratti, 2014), the K⁺ ionophore valinomycin and K⁺/H⁺ exchangers salinomycin and nigericin, all shown to reach the mitochondrial inner membrane (e.g., Managò et al., 2015 and references therein), were exploited (Figure 1A). In addition, (3-(4-(4-((7-oxo-7H-furo[3,2-g]benzopyran-4-yl)oxy)butoxy)phenyl)propyl)triphenyl phosphonium iodide (PAPTP) and (3-(((4-(4-((7-oxo-7H-furo[3,2-g]benzopyran-4-yl)oxy)butoxy)phenoxy)carbonyl) amino) propyl) triphenylphosphonium iodide (PCARBTP), two recently described specific mitochondria-targeted derivatives of 5-(4-Phenoxybutoxy)psoralen (PAP-1), were used (Figure 1A). PAP-1 is an inhibitor of the K⁺ channel

Kv1.3 that is expressed in different cells (Perez-Verdaguer et al., 2016), including HEK293 (Ponce et al., 2018). Both compounds were shown to inhibit the mitochondria-located Kv1.3 to trigger mitochondrial ROS release and changes in mitochondrial membrane potential (Leanza et al., 2017).

In our experiments, all of the above compounds significantly reduced the Wnt reporter activity (Figure 1A), while the luciferase enzymatic activity itself was not affected (Figure S1C). Similar results were obtained when Wnt signaling was induced by constitutively active β-catenin or by Wnt3A ligand expression (Figures S1D and S1E). While the K⁺ ionophores act both at the plasma membrane and the mitochondrial inner membrane, the specificity of the mitochondria-Wnt axis was evident from experiments using respiratory chain inhibitors. Comparison of the Wnt-reducing effects of the membrane permeant Kv1.3 inhibitors with those of the membrane impermeant Kv1.3 blockers (margatoxin [MgTx], stichodactyla toxin [ShK], and charybdotoxin [ChTx]), which did not affect Wnt signaling (Figure 1A), also strongly points to a mitochondria-Wnt axis. The drugs specifically affected Wnt signaling, since neither Notch nor the Hippo pathways were modulated by the used compounds (Figures S1F and S1G). This also further indicates the lack of toxicity of the drugs at the concentrations used. Downregulation of Wnt signaling was also confirmed by western blot; the protein levels of β-catenin and two of its target genes, lymphoid enhancer-binding factor 1 (LEF1) and the receptor tyrosine kinase MET, were reduced (Figures 1B and 1C). Downregulation of the gene transcription of two Wnt-dependent genes, Cyclin D1 and Dickkopf 1 (DKK1), was also observed, while transcription of β-catenin remained unaffected (Herbst et al., 2014) (Figure S1H).

To confirm our findings also in in vivo experiments, we used the well-established Tg(7xTCFX.lasiam:EGFP)ia4 zebrafish reporter line for canonical Wnt signaling (Moro et al., 2012). Sublethal doses of the above compounds significantly diminished Wnt reporter activity, with similar effects to XAV939 (Figures 1D and 1E), and the β-catenin protein level was reduced in developing embryos upon treatment (Figure 1F). In accordance with reduced Wnt signaling, the sagittal axis of the treated larvae was shortened in comparison to the control animals, phenocopying the well-known effect of the Wnt inhibitor XAV939 on embryo development (Shimizu et al., 2012) (Figure 1D).

Figure 1. Mitochondrial Fitness Fine-Tunes Wnt Signaling in Human Embryonic Kidney HEK293 Cells and in Wnt-Dependent Reporter Zebrafish

(A) Canonical Wnt signaling activity based on TCF-LEF-dependent transcription was assayed in HEK293 cells. These cells were either left untreated or Wnt signaling was enhanced using 3 μM CHIR99021 (CHIR). Cells were then treated for 8 h with the following compounds: 0.1% DMSO, as negative control; 10 μM XAV939 (XAV) as positive control; MgTx, ShK, ChTx (1 μM); PAP-1 (20 μM) + cyclosporin H (CSH) (4 μM); 1 μM PAPTP, 5 μM PCARBTP; 5 μM salinomycin (Salino), 0.5 μM nigericin (Nige), 1 μM valinomycin (Valino); and 2 μM FCCP; 5 μM rotenone (Rot), 0.5 mM TTFA, 1.8 μM antimycin A (Anti), and 1.2 μM oligomycin (Oligo). The luciferase signal was normalized with respect to the signal given by β-gal, which was co-transfected with TOPflash plasmid. The values are reported as the percentage of luciferase signal related to the "ref." Values are means ± SEMs (n = 8).

(B and C) Reduction of protein levels of β-catenin and its target genes LEF1 and MET are shown in representative western blots (B). Densitometric analysis (n = 6; means ± SEMs) is reported in (C).

(D and E) GFP fluorescent zebrafish Tg(7xTCFX.lasiam:EGFP)ia4 Wnt-dependent reporter fishes were treated for 15 h with the following compounds: DMSO 0.2%, 20 μM XAV, 1 μM Salino, 1.5 μM PAPTP, 5 μM PCARBTP, 50 μM TTFA, and 0.12 μM Oligo. Representative bright-field and epifluorescence microscopy images are reported in (D), while fluorescence quantification is shown in (E) (means ± SEMs). The numbers reported on the graph represent the number of zebrafish embryos treated for each condition. Bars, 1.5 mm.

(F) Zebrafish β-catenin (Zβ-catenin) protein level from embryos treated as (D) and (E) was determined by western blot. The quantification is reported below. The values are indicated as the percentage of the "ref" (n = 3; means ± SEMs).

Statistical significance (ANOVA) was determined as *p < 0.05, **p < 0.01, and ***p < 0.001.
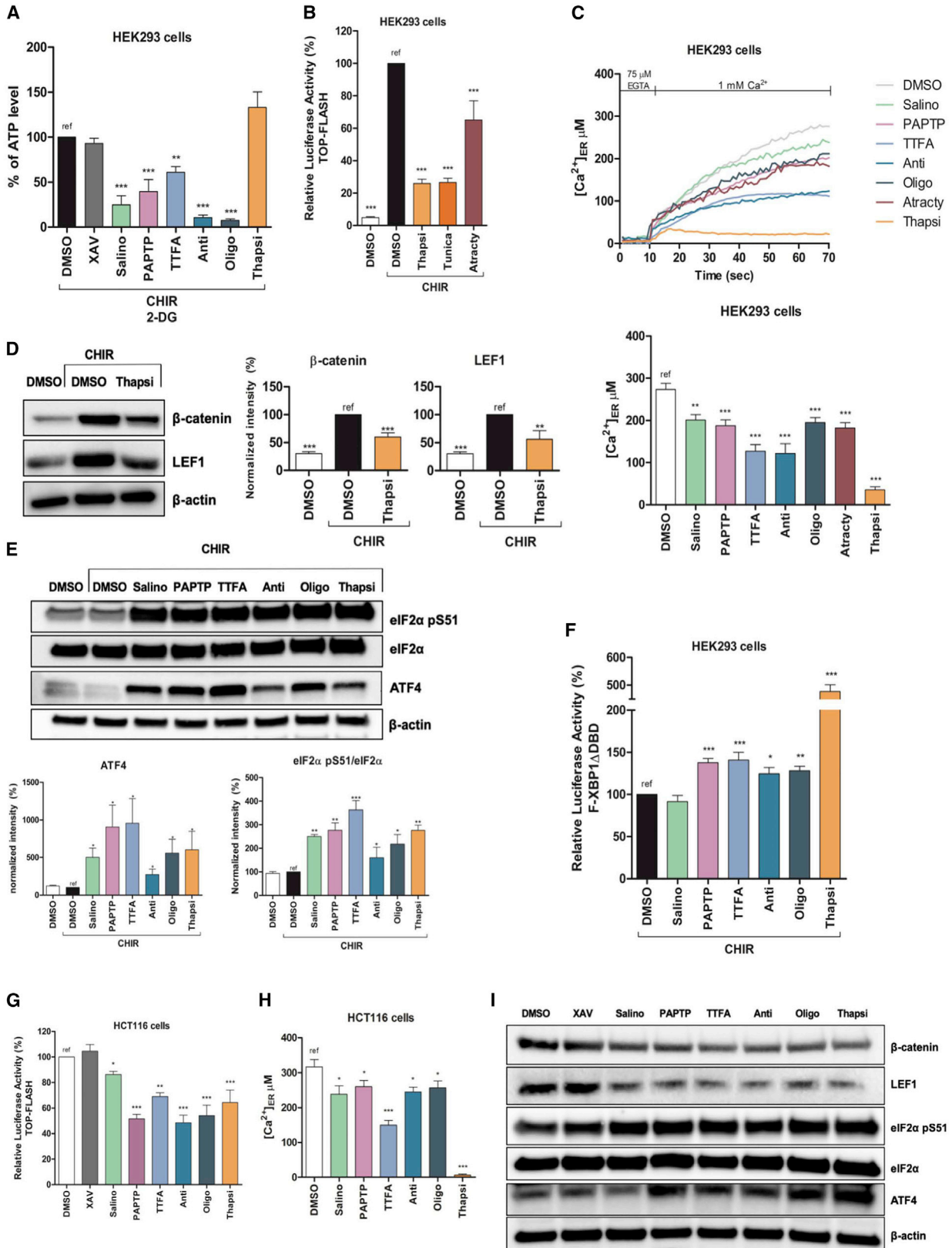
(legend on next page)

As a control of the specificity of the effects of the drugs on Wnt signaling, three further pathways were studied *in vivo*: (1) Sonic Hedgehog (Shh), an important signaling pathway involved in cellular specification and proliferation (Figure S1I); (2) oligodendrocyte transcription factor 2 (Olig2), required for oligodendrocyte and motor neuron specification in the spinal cord (Figure S1J); and (3) the erythroid transcription factor Gata 1 (Figure S1K), which plays a critical role in the normal development of hematopoietic cell lineages. In none of these cases did downregulation occur upon treatment, indicating *in vivo* specificity as well as a lack of toxicity of the drugs at the concentrations used.

All of these chemicals caused similar *in vitro* and *in vivo* effects on Wnt signaling activity; however, at the molecular level, they have very different actions, leading us to wonder what common mechanism could be responsible for the regulation of Wnt. The depolarization of the mitochondrial membrane potential (observed only for valinomycin, PAPTP, PCARBTP, FCCP, and antimycin A, not for salinomycin and nigericin) or matrix acidification (takes place only with salinomycin, nigericin, PAPTP, and antimycin) is not a common effect of these drugs, according to previous data (e.g., Forkink et al., 2015; Leanza et al., 2017; Managò et al., 2015). Hydrogen peroxide was shown to activate canonical Wnt signaling (Funato et al., 2006), but in our case, some of the drugs induce ROS release (antimycin A, valinomycin, FCCP, PAPTP, PCARBTP; Leanza et al., 2017; Managò et al., 2015), while others do not (nigericin or salinomycin; Managò et al., 2015) within the examined timescale. Further possible links, such as β-catenin activation by serine 552 phosphorylation via protein kinase A (PKA) or serine-threonine protein kinase Akt (Lee et al., 2010) (Figure S2A) and fatty acid biosynthesis or oxidation as the readout of AMP kinase (AMPK) activity that is regulated by the cytoplasmic ATP:AMP ratio (Ha et al., 1994) (Figure S2B), have been explored. However, none of these modulatory events changed with any of the drugs that were able to decrease Wnt signaling.

All of the drugs, except XAV939 and thapsigargin, that were used as negative controls, however, reduced mitochondrial ATP production (Figure 2A) (assessed using 2-deoxyglucose to block the contribution of glycolysis to the overall ATP level in the cells). This result led us to hypothesize that the effects on Wnt were mediated by reduced mitochondria-derived ATP levels independently of the overall ATP concentration within the cells. In agreement with our hypothesis, atractyloside, an inhibitor of the adenine nucleotide transporter (ANT) that exports synthetized ATP from the mitochondrial matrix, was able to reduce Wnt signaling even when glycolysis was active (Figure 2B). Thanks to the crucial cross-talk between mitochondria and the endoplasmic reticulum (ER) (Rizzuto et al., 2012), specifically the mitochondrial ATP pool seems to be important for the activity of the sarcoplasmic/endoplasmic reticulum Ca^{2+}-ATPase (SERCA), since its function was shown to be inhibited by the reduced amount of mitochondrial ATP in the interstitial spaces in the mitochondria-associated membranes (MAMs) (De Marchi et al., 2011; Madreiter-Sokolowski et al., 2016). In accordance with the expected reduced activity of SERCA, we observed a reduction in calcium (Ca^{2+}) levels in the endoplasmic reticulum upon treatment with the drugs able to reduce mitochondrial ATP production or its export to the cytosol (atractyloside) (Figure 2C), without modulation of the non-canonical Wnt/Ca^{2+} pathway (Figure S2C). Independent of the addition of 2-deoxyglucose, oligomycin and PAPTP reduced Ca^{2+} uptake in the endoplasmic reticulum, further underlining the importance of mitochondrial ATP in this pathway (Figure S2D). The widely used endoplasmic reticulum-targeted aequorin was exploited to monitor dynamic changes in free Ca^{2+} concentration in the endoplasmic reticulum of intact cells (Montero et al., 1995).

Endoplasmic reticulum function modulators thapsigargin and tunicamycin equally elicited Wnt downregulation (Figures 2B and 2D). Thapsigargin disrupts the Ca^{2+} storage of endoplasmic reticulum by blocking SERCA and thus Ca^{2+} reuptake into the endoplasmic reticulum lumen, thereby depleting endoplasmic reticulum Ca^{2+} (Figure 2C). Tunicamycin, a highly specific endoplasmic reticulum stress inducer, was also able to decrease Wnt signaling (Figure 2B). To further validate the importance of the endoplasmic reticulum-mitochondria proximity in this pathway, we transiently overexpressed Mitofusin2 (MFN2) in HeLa cells

Figure 2. Mitochondria-Wnt Signaling Axis Is Mediated by Reduced Mitochondrial ATP Synthesis and Endoplasmic Reticulum (ER) Stress Induction in HEK293 and Colon Cancer Cells

(A) Mitochondrial ATP content was measured in HEK293 cells treated as in Figure 1A, but in a medium containing 5 mM 2-deoxyglucose (2-DG). Thapsigargin (Thapsi) was used at 1 μM (n = 4; means ± SEMs).

(B) Canonical Wnt signaling activity was assayed in HEK293 cells as in Figure 1A. Cells were treated with 1 μM Thapsi, 0.5 μg/mL tunicamycin (Tunica), or 10 μM atractyloside (Atracty).

(C) Endoplasmic reticulum Ca^{2+} levels in HEK293 cells treated for 6 h as in (B) or Figure 1A. Representative traces of the endoplasmic reticulum Ca^{2+} reuptake are shown in the upper panel, while the quantification at steady state is reported at bottom (n = 3; means ± SEMs). The values are reported as Ca^{2+} concentrations, and analysis is related to the "ref."

(D) β-Catenin and LEF1 reduction was measured in HEK293 cells by western blot after treatment with Thapsi. A representative blot is shown at left, while quantification is reported at right (n = 4; means ± SEMs).

(E) Induction of endoplasmic reticulum stress was shown in HEK293 cells by increased phosphorylation of eIF2α and enhanced expression of ATF4 treated as in (D) and Figure 1A. A representative blot is shown in the upper panel, while the quantification related to the "ref" is reported at bottom (n = 3; means ± SEMs).

(F) Endoplasmic reticulum stress induction was studied in HEK293 cells transfected with a F-XBP1ΔDBD plasmid and treated as in (B) and Figure 1A with a luciferase reporter assay. The values are reported as the percentage of luciferase signal related to the "ref" (n = 5; means ± SEMs).

(G) Canonical Wnt signaling activity based on TCF-LEF-dependent transcription was assayed in HCT116 cells as in Figure 1A for 8 h, without the addition of CHIR (n = 3; means ± SEMs).

(H) Endoplasmic reticulum Ca^{2+} levels in HCT116 cells after a 6-h treatment with the indicated compounds (as in G). Analysis as in (C) (n = 3, means ± SEMs).

(I) β-Catenin and LEF1 reduction and endoplasmic reticulum stress induction were measured in HCT116 cells by western blot after treatment as in (G). Quantification is reported in Figure S2G.

Statistical significance (ANOVA) was determined as *p < 0.05, **p < 0.01, and ***p < 0.001.
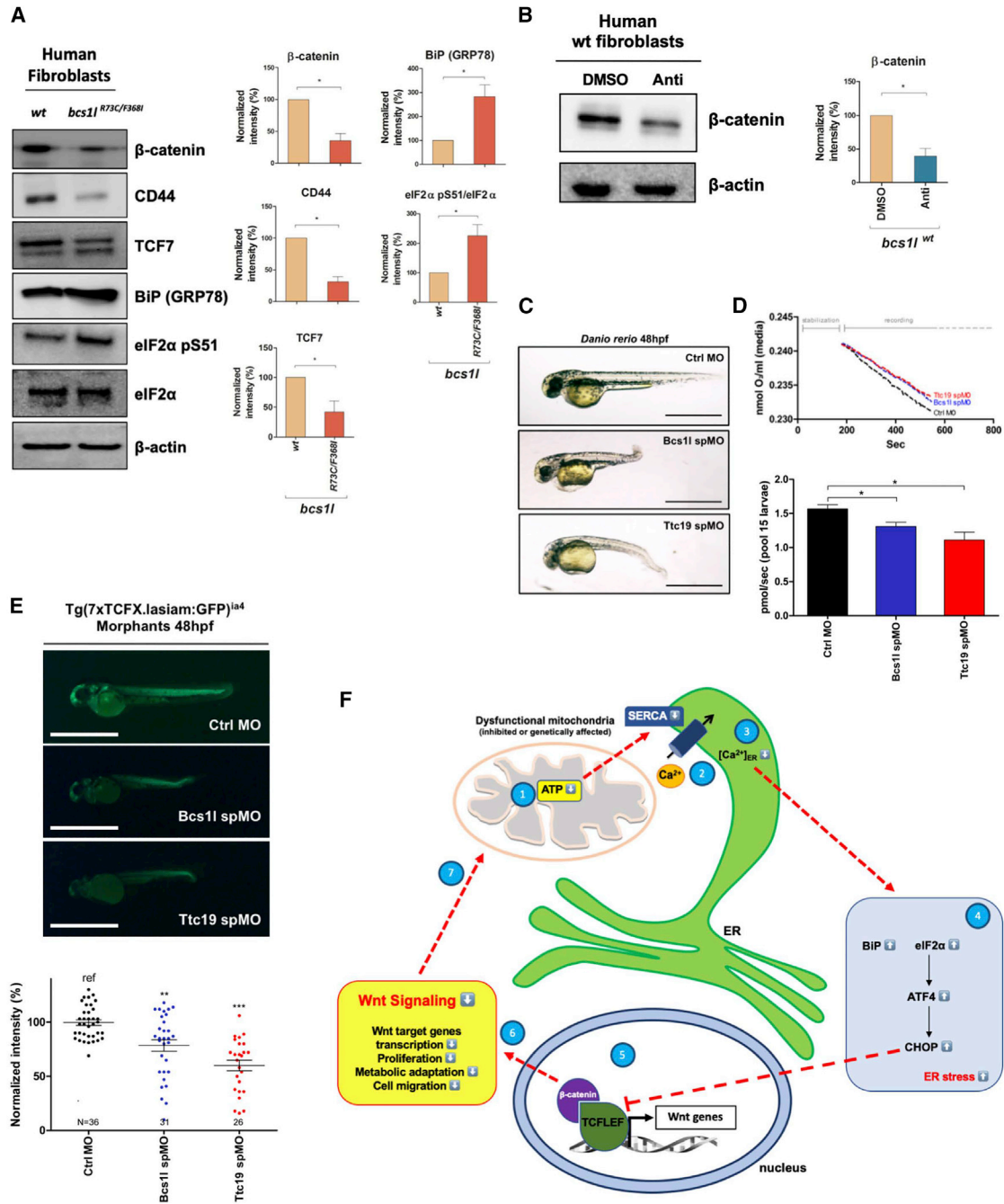
Figure 3. Mitochondrial Fitness Fine-Tunes Wnt Signaling in Human Fibroblasts and in Respiratory Chain Complex III Deficiency Zebrafish Models

(A) Reduction of the protein levels of β-catenin and its target genes TCF7 and CD44 and endoplasmic reticulum stress induction was observed in human immortalized fibroblasts. Protein extracts obtained from healthy donors (WT) or GRACILE patients (*bcs1l*[R73C/F368I]) were used. A representative blot and quantification are shown (left and right, respectively; n = 3; means ± SEMs).

(B) Total protein extracts from human immortalized fibroblasts from healthy donors treated overnight with 0.2% DMSO or 1 μM Anti were analyzed by western blot. The quantification is shown at right (n = 3; means ± SEMs).

(C) Transient knockdown of the respiratory chain complex III was performed by two independent splicing morpholinos against Ttc19 and Bcs1l mRNAs (Ttc19 spMO and Bcs1l spMO); a standard control morpholino was also used. Bright-field images of morphants are reported. Bars, 1 mm.

(D) Respiratory efficiency of morpholino-injected embryos (pool of 15 embryos) was analyzed by the Oxygraph+ instrument. Oxygen concentration in the medium and the consumption rate are plotted.

(Figure S2E). MFN2 overexpression enhanced the number of endoplasmic reticulum-mitochondria contact sites as documented by the quantification of green fluorescent dots (Figure S2F) (Cieri et al., 2018; Csordás et al., 2010; Giacomello et al., 2010). Under the same MFN2 overexpression conditions, we monitored endoplasmic reticulum Ca^{2+} uptake, as in Figure 2C (Figure S2G). We found that HeLa cells overexpressing MFN2 reached a higher plateau level of endoplasmic reticulum Ca^{2+} in the lumen than mock transfected cells, indicating that enhanced endoplasmic reticulum-mitochondria tethering is able to support SERCA pump activity in refilling endoplasmic reticulum stores. No variations in SERCA or luminal endoplasmic reticulum Ca^{2+}-buffering proteins (e.g., calreticulin, calnexin) expression have been observed upon the transient overexpression of MFN2 (Figure S2E).

The reduced Ca^{2+} content in the endoplasmic reticulum resulted in endoplasmic reticulum stress, as expected (Jung and Choi, 2016; Savignac et al., 2014) and as indicated in our experiments by classical endoplasmic reticulum stress-related events such as increased phosphorylation of the eukaryotic initiation factor 2 (eIF2α), upregulation of both activating transcription factor 4 (ATF4) and binding immunoglobulin protein (BiP/GRP78, an endoplasmic reticulum chaperone), and by an increased X-box-binding protein 1 (XBP-1) transcriptional activity (Figures 2E, 2F, and S2H) (for review, see, e.g., Rozpedek et al., 2016). Endoplasmic reticulum stress has previously been shown to trigger Wnt signaling downregulation, since ATF4 enhances the expression of transcription factors, including CHOP (CCAAT/enhancer-binding protein homologous protein)/GADD153 (growth arrest and DNA damage-inducible protein) (Wek et al., 2006). CHOP functions as a specific inhibitor of Wnt-T cell factor (TCF) signaling (e.g., Horndasch et al., 2006; Verras et al., 2008), since it prevents the binding of TCF to its DNA recognition site. Even though the Akt kinase expression level did not change, endoplasmic reticulum stress-induced phosphorylation of Akt at serine 473 occurred, as expected (Yung et al., 2011) (Figures S3A–S3C). Akt activation, however, did not significantly affect GSK3β expression and phosphorylation when Wnt signaling was enhanced by the ligand Wnt3a (Figures S2A–S2C).

As Wnt signaling is constitutively upregulated in colon cancers (thus, no activation by CHIR99021 is required), the HCT116 colon cancer line was used to show that mitochondrial ATP depletion (Figure S4A) induced reduction in the calcium levels in the endoplasmic reticulum set by SERCA (Figure 2H) and endoplasmic reticulum stress (Figures 2I and S4C). All of the drugs used reduced Wnt signaling in these tumor cells already at sublethal concentrations (Figure S4B) and within 8 h after application (Figures 2G, 2I, and S4C). In these cells, the effects of XAV939

and the other compounds were less pronounced on the β-catenin level compared to HEK293 cells (Li et al., 2015), most likely due to a mutation in the β-catenin itself in HCT116 (Ichimanda et al., 2018; Shikata et al., 2017). Similar results were obtained in another colon cancer line, DLD1, characterized by constitutively active Wnt signaling due to a truncation in adenomatous polyposis coli (APC) (Homfray et al., 1998; Kishida et al., 1998), concerning viability upon treatment (Figure S4D), reduction of Wnt signaling (Figures S4E and S4G), ATP depletion (Figure S4F), and endoplasmic reticulum stress (Figure S4G).

To genetically validate the direct functional epistasis between mitochondrial function and endoplasmic reticulum stress-Wnt signaling, we used fibroblasts obtained from a patient with GRACILE syndrome caused by respiratory chain complex III deficiency. This patient is characterized by composed heterozygous mutations of $bcs1l$ ($bcs1l^{R73C/F368I}$), encoding an assembly factor of complex III (Fernandez-Vizarra et al., 2007). These cells exhibited an increased endoplasmic reticulum stress (Figure 3A) and downregulated β-catenin, its related transcription factor TCF7, and CD44 (Wnt targets; Herbst et al., 2014) protein levels compared to normal fibroblasts (Figure 3A), which show a similar phenotype upon treatment with the complex III inhibitor antimycin A (Figure 3B).

To validate and generalize this observation also in vivo, we generated two independent zebrafish models for complex III diseases. By using morpholino-mediated transient knockdown of two previously identified complex III assembly factors, Bcs1l or Ttc19 (Bottani et al., 2017; Ghezzi et al., 2011), we observed reduced respiration as expected (Figure 3D) in addition to sagittal axis shortening, tail and craniofacial deformity, and lower pigmentation in comparison to controls (Figure 3C). In both cases, statistically significant reduction in Wnt signaling was evident (Figure 3E), confirming in vivo that the genetic modulation of complex III efficiency downregulates Wnt signaling.

The data above suggest that mitochondrial function and ATP production, by maintaining Ca^{2+} stores in the endoplasmic reticulum, relieve endoplasmic reticulum stress and enable efficient Wnt signaling (Figure 3F). To validate this hypothesis, we reinstalled mitochondrial ATP synthesis by supplementing cells with phosphoenolpyruvate (PEP) or creatine (Figure 4A), and we observed rescued Wnt activity in cells where the ATP level was markedly reduced by treatment with PAPTP (Figures 2A and 4B). Reducing endoplasmic reticulum stress by 4-phenyl butyric acid (4-PBA) (Ben Mosbah et al., 2010) equally re-activated Wnt, even in the presence of PAPTP (Figure 4B). Finally, treatment with phosphoenolpyruvate, creatine, or 4-PBA of $bcs1l^{R73C/F368I}$ fibroblasts rescued not only mitochondrial ATP content (phosphoenolpyruvate and creatine; Figure 4C) but

(E) Knock down of the respiratory complex III was performed in Tg(7xTCFX.lasiam:GFP)^{ia4} by Ttc19 spMO and Bcs1l spMO and compared to the control. GFP epifluorescence quantification was reported in the graph below; dots and numbers represent treated embryos (means ± SEMs). Statistical significance (ANOVA) was determined as *$p < 0.05$, **$p < 0.01$, and ***$p < 0.001$). Bars, 1 mm.

(F) Mito-Wnt axis is an important pathway in which mitochondrial dysfunction (1), due to mutated genes or to pharmacological treatment, leads to reduced mitochondrial ATP synthesis, which directly affects Ca^{2+} uptake by regulating SERCA in the endoplasmic reticulum (2). This in turn decreases Ca^{2+} levels in the endoplasmic reticulum (3), leading to endoplasmic reticulum stress induction by the phosphorylation of eIF2α and activation of its downstream factors ATF4 and CHOP (4), which are able to modulate Wnt signaling by a still-debated mechanism (5). This modulation could regulate several downstream events such as gene transcription of Wnt target genes, leading to the control of cell proliferation, metabolic adaptation, and cell migration, in particular, modulating cancer development and the spreading of metastasis (6). Finally, a possible feedback mechanism of reduced Wnt signaling can further regulate mitochondrial activity (7). As indicated by experiments shown in Figure S2D, glycolysis also contributes to the regulation of Ca^{2+} uptake into the endoplasmic reticulum.
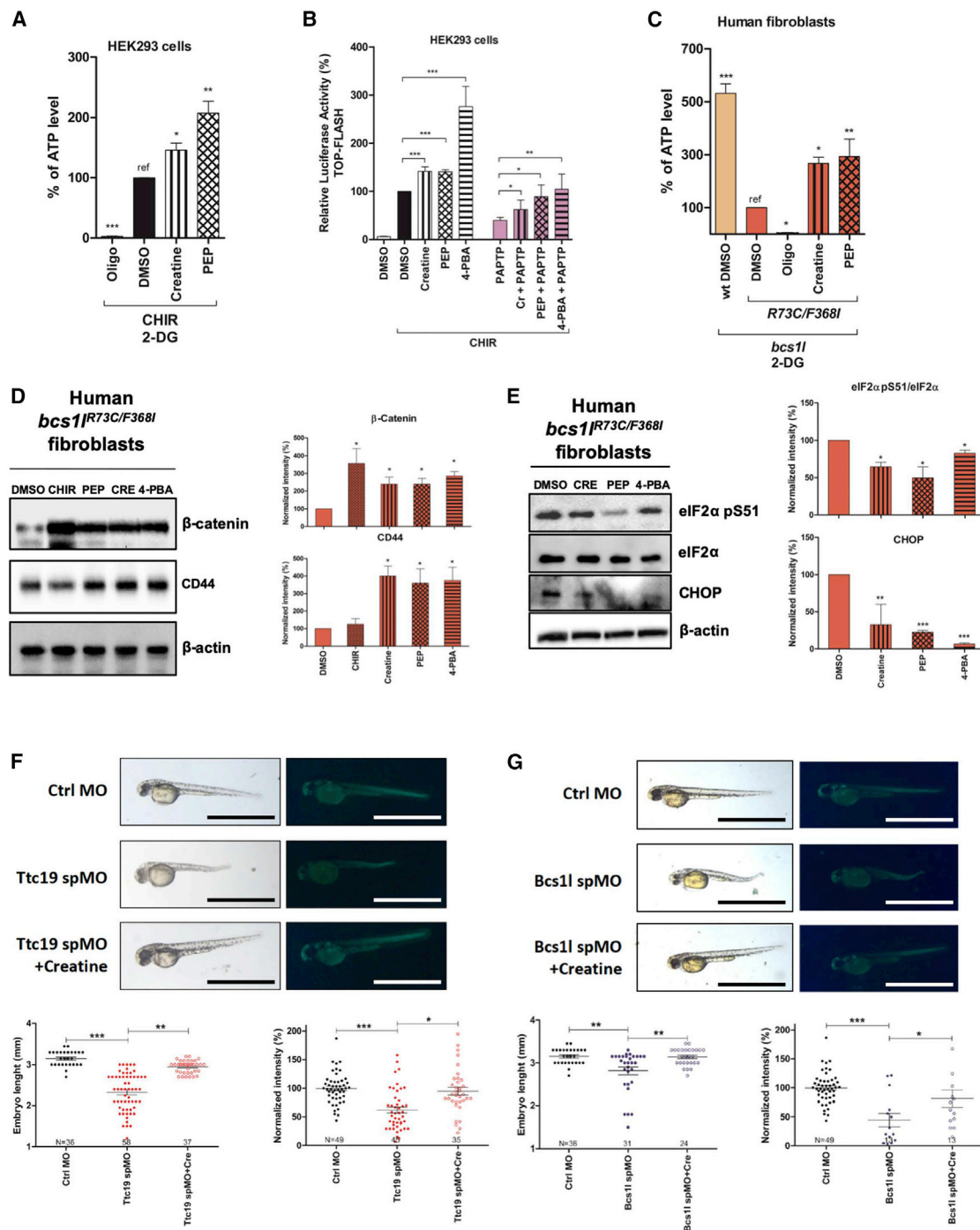
Figure 4. Increased Mitochondrial ATP Production or Endoplasmic Reticulum Stress Inhibition Rescues Wnt Signaling

(A) Mitochondrial ATP content was measured in HEK293 cells, after treatment with 1 mM creatine (CRE) or 60 μM phosphoenolpyruvate (PEP) for 30 min. Furthermore, Wnt signaling was induced by co-administration of 3 μM CHIR. The analysis was conducted as in Figure 2A (n = 3; means ± SEMs).

(B) Canonical Wnt signaling activity based on TCF-LEF-dependent transcription was assayed in HEK293 cells, as in Figure 1A. Cells were pre-treated for 30 min with CRE or phosphoenolpyruvate or for 2 h with 0.5 mM of the endoplasmic reticulum stress inhibitor 4-phenyl butyric acid (4-PBA) before addition and incubation with or without 1 μM PAPTP for a further 8 h (n = 3; means ± SEMs).

(C) Mitochondrial ATP was measured and analyzed in human immortalized fibroblasts from healthy donors (WT) or a GRACILE patient (n = 3). Cells were pre-treated as in (A).

(D) β-Catenin and CD44 recovery were measured in bcs1l^R73C/F368I fibroblasts by western blot after treatment with the following compounds: 3 μM CHIR, 1 mM CRE, 0.6 mM phosphoenolpyruvate, or 0.5 mM 4-PBA.

(legend continued on next page)

also increased the protein levels of β-catenin and CD44 (Figure 4D) and reduced endoplasmic reticulum stress (Figure 4E). Finally, we show that in our zebrafish models, the recovery of Wnt signaling and of the wild-type (WT)-like phenotype and length can be achieved by the administration of creatine *in vivo* (Figures 4F and 4G).

DISCUSSION

The data in the present paper indicate the existence of a mitochondrial-Wnt signaling axis, in which mitochondrial ATP plays a crucial role in fine-tuning this important pathway by allowing correct SERCA function and appropriate loading of endoplasmic reticulum with Ca^{2+} (Figure 3F) to avoid endoplasmic reticulum stress, which in turn reduces Wnt signaling. The data obtained with the patients' fibroblasts are in agreement with the pharmacological data in WT cells, indicating that a markedly reduced mitochondrial ATP level, which can be observed in GRACILE syndrome fibroblasts due to impaired complex III function, is linked to increased endoplasmic reticulum stress and reduced Wnt signaling.

The experimental results reported here show that perturbation of mitochondrial function using a number of inhibitors can cause decreased Wnt activity both *in vitro* and *in vivo*. Wnt signaling downregulation is not due to a general toxicity or to an endoplasmic reticulum stress-linked inhibition of transcription or translation, since cell survival was not affected and β-catenin transcription itself was not decreased upon treatment; several different proteins such as actin, GSK3α, GSK3β, and Wnt5 were present at the same level in both untreated and treated samples. In the present study, we investigated the short-term effects of different compounds used at sublethal concentrations. We cannot exclude, however, that at much higher concentrations and/or longer incubation times the drugs may induce mitochondrial damage and Wnt signaling may increase as part of an adoptive response, as suggested by Bernkopf et al. (2018). These investigators observed an increased Wnt signaling 72 h after the treatment of the cells with a very high dose (100 μM) of the uncoupler carbonyl cyanide *m*-chlorophenyl hydrazone (CCCP) (in contrast to the 2 μM FCCP used here). It must be mentioned that higher concentrations of the drugs than those used in this study may also trigger apoptosis (e.g., Leanza et al., 2017; Managò et al., 2015).

Some of the drugs used here were shown to have beneficial effects in the context of cancer development, in which Wnt signaling plays a crucial role. Oligomycin 10 μM was shown to inhibit mammosphere formation in MCF7 breast cancer cells (De Luca et al., 2015), and a sublethal dose (0.5 mg/kg) of oligomycin was able to prevent K-Ras expression-induced tumor relapse of pancreatic ductal adenocarcinoma even *in vivo* (Viale et al., 2014). Valinomycin, salinomycin, and nigericin were re-

ported to inhibit cancer stem cell survival (Managò et al., 2015). PAPTP and PCARBTP were shown to induce a drastic reduction in tumor size *in vivo* in the case of melanoma and pancreatic ductal adenocarcinoma at 5 nmol/g mouse (Leanza et al., 2017). While previous sporadic observations linked the effect of some of the drugs used here (e.g., potassium ionophores) to Wnt signaling, the present work shows that such regulation takes place efficiently *in vivo* and provides a rationale for a common mechanism of action.

Our results indicate that SERCA activity is crucial for Wnt signaling both *in vitro* and *in vivo*, in agreement with previous suggestions (Lu and Carson, 2009; Lu et al., 2011). ATP regulates SERCA function in the mitochondria-associated membranes (De Marchi et al., 2011; Madreiter-Sokolowski et al., 2016), and we show that mitochondrial ATP is involved in the proposed pathway, since both endoplasmic reticulum calcium level and Wnt signaling are significantly reduced even when glycolytic ATP is available, but ATP export from the matrix is blocked using atractyloside, an ANT inhibitor. Our results also suggest that the genetic modulation of endoplasmic reticulum-mitochondria tethering by overexpressing MFN2 increases the endoplasmic reticulum Ca^{2+} content. Although this effect apparently cannot be ascribed to an increased SERCA expression and/or decreased expression of some of the endoplasmic reticulum proteins involved in Ca^{2+} buffering, possible changes (e.g., in the activity of SERCA depending on the expression of MFN2) cannot be excluded. Therefore, the precise molecular mechanism that can explain our observation needs to be further investigated.

In our experiments, a decrease in SERCA function upon reduction of ATP supplied by mitochondria leads to endoplasmic reticulum stress. Nevertheless, we cannot exclude that other factors (e.g., mitochondria-released metabolites) also contribute to the regulation of this chain of events. Increased endoplasmic reticulum stress was previously linked to the inhibition of Wnt signaling via CHOP (Horndasch et al., 2006; Verras et al., 2008) and has been confirmed also by several other studies (e.g., Huang et al., 2018; Shen et al., 2014), but the exact mechanism linking these events is still debated. Endoplasmic reticulum stress was proposed to inhibit Wnt signaling by interfering with the glycosylation of Wnt ligands (Verras et al., 2008), but recent data point to the endoplasmic reticulum stress-triggered loss of Wnt signaling occurring at a level downstream of β-catenin (van Lidth de Jeude et al., 2017). Thus, further work will be required to understand the fine details of the endoplasmic reticulum stress-Wnt downregulation axis.

Mitochondrial fitness and metabolites are emerging as master regulators of crucial cellular functions and differentiation. Succinate has recently been discovered to drive thermogenesis in brown fat tissues (Mills et al., 2018). Mitochondrial ROS regulates myc signaling (Zhang et al., 2017), while mitochondrial

---

(E) Endoplasmic reticulum stress rescue was measured in *bcs1l*[R73C/F368I] fibroblasts. Representative blots are shown at left, while the quantification is reported at right (n = 3; means ± SEMs).

(F and G) Zebrafish morphants for Ttc19 (F) and Bcs1l (G) were obtained as in Figures 3C and 3E. Bright-field images of morphants as well as reporter GFP epifluorescence are shown. The sagittal length and GFP epifluorescence quantification of embryos are reported in the graph below (means ± SEMs; dots and numbers represent treated embryos). Bars, 1.5 mm.

Statistical significance (ANOVA) was determined as *$p < 0.05$, **$p < 0.01$, and ***$p < 0.001$.

morphology affects Notch signaling (Kasahara et al., 2013). Glucose metabolism was shown to regulate Yes-associated protein (YAP)/transcriptional co-activator with PDZ-binding motif (TAZ), key transcription factors affecting tumor cell proliferation and aggressiveness (Enzo et al., 2015). Finally, a very recent report showed that the knockdown of transcription factor A, mitochondrial (TFAM), a transcription factor that is essential for mtDNA replication, resulted in the decreased expression of genes downstream of Wnt/β-catenin signaling (Wen et al., 2019). Our observations can be of relevance in the context of cancer therapy, since the induction of mitochondrial dysfunction leading to a reduced mitochondrial ATP level and possibly to the consequent inhibition of Wnt-β-catenin signaling can be beneficial against Wnt-dependent cancer progression (Ishii et al., 2012), even at sublethal concentrations, either alone or in combination therapy with currently used chemotherapeutics (Kruspig et al., 2016).

The observation that phosphoenolpyruvate and creatine are able to increase Wnt signaling by increasing the mitochondrial ATP level and can rescue the phenotype of complex III disease zebrafish models can be of clinical relevance in the context of neurogenesis following injury. The view that increasing neurogenesis through activating the Wnt signaling pathway in depression can preserve brain function is emerging (Lee and Baek, 2017). Benefits of creatine supplementation have been reported for depression and other CNS diseases (Pazini et al., 2017). A very recent paper highlighted that creatine supplementation can prevent, via activation of the Wnt/GSK3β/β-catenin pathway, chronic mild stress-induced decreases in hippocampal neurogenesis (Leem et al., 2018). However, the underlying molecular mechanism was not addressed in these papers. Thus, the information reported in the present article can be of relevance in the context of both cancer and neurogenesis. In addition, it suggests that creatine supplementation may have beneficial effects in the case of complex III disease patients, who can present with severe neurological deficits.

STAR★METHODS

Detailed methods are provided in the online version of this paper and include the following:

- KEY RESOURCES TABLE
- LEAD CONTACT AND MATERIALS AVAILABILITY
- EXPERIMENTAL MODEL AND SUBJECT DETAILS
  - ○ Animal studies
  - ○ Cell cultures
- METHOD DETAILS
  - ○ Reagents
  - ○ Protein lysates and electrophoresis
  - ○ Western Blotting
  - ○ Real-Time PCR
  - ○ MTS assay
  - ○ Luciferase assays
  - ○ Determination of ATP concentration
  - ○ *In vivo* experiments
  - ○ Morpholinos injection, Oxygraph analysis and rescue
  - ○ ER-mitochondria Contact Site Analysis
  - ○ Calcium uptake measurements
- QUANTIFICATION AND STATISTICAL ANALYSIS
- DATA AND CODE AVAILABILITY

AUTHOR CONTRIBUTIONS

Conceptualization, L.L. and I.S.; Methodology, L.L., R.P., M. Bachmann, R.C., I.S., T.C., and M. Brini; Investigation, R.C., R.P., M. Bachmann, M.V., G.D.M., R.Q.-C., T.C., and F.V.; Resources, G.S., M. Zoratti, F.A., A.M., M. Zeviani, and C.P.; Writing – Original Draft, I.S., L.L., S.D., E.M., L.S., and M. Zoratti; Funding Acquisition, I.S., L.L., and M. Zoratti; Supervision, L.L. and I.S.

DECLARATION OF INTERESTS

The authors declare no competing interests.

REFERENCES

Azzolin, L., Zanconato, F., Bresolin, S., Forcato, M., Basso, G., Bicciato, S., Cordenonsi, M., and Piccolo, S. (2012). Role of TAZ as mediator of Wnt signaling. Cell *151*, 1443–1456.

Azzolin, L., Panciera, T., Soligo, S., Enzo, E., Bicciato, S., Dupont, S., Bresolin, S., Frasson, C., Basso, G., Guzzardo, V., et al. (2014). YAP/TAZ incorporation in the β-catenin destruction complex orchestrates the Wnt response. Cell *158*, 157–170.

Ben Mosbah, I., Alfany-Fernández, I., Martel, C., Zaouali, M.A., Bintanel-Morcillo, M., Rimola, A., Rodés, J., Brenner, C., Roselló-Catafau, J., and Peralta, C. (2010). Endoplasmic reticulum stress inhibition protects steatotic and non-steatotic livers in partial hepatectomy under ischemia-reperfusion. Cell Death Dis. *1*, e52.

Bernkopf, D.B., and Behrens, J. (2018). Cell intrinsic Wnt/β-catenin signaling activation. Aging (Albany N.Y.) *10*, 855–856.

Bernkopf, D.B., Jalal, K., Brückner, M., Knaup, K.X., Gentzel, M., Schambony, A., and Behrens, J. (2018). Pgam5 released from damaged mitochondria induces mitochondrial biogenesis via Wnt signaling. J. Cell Biol. *217*, 1383–1394.

Bottani, E., Cerutti, R., Harbour, M.E., Ravaglia, S., Dogan, S.A., Giordano, C., Fearnley, I.M., D'Amati, G., Viscomi, C., Fernandez-Vizarra, E., and Zeviani, M. (2017). TTC19 Plays a Husbandry Role on UQCRFS1 Turnover in the Biogenesis of Mitochondrial Respiratory Complex III. Mol. Cell *67*, 96–105.e4.

Brini, M., Marsault, R., Bastianutto, C., Alvarez, J., Pozzan, T., and Rizzuto, R. (1995). Transfected aequorin in the measurement of cytosolic Ca2+ concentration ([Ca2+]c). A critical evaluation. J. Biol. Chem. *270*, 9896–9903.

Chrétien, D., Bénit, P., Ha, H.H., Keipert, S., El-Khoury, R., Chang, Y.T., Jastroch, M., Jacobs, H.T., Rustin, P., and Rak, M. (2018). Mitochondria are physiologically maintained at close to 50 °C. PLoS Biol. *16*, e2003992.

Cieri, D., Vicario, M., Giacomello, M., Vallese, F., Filadi, R., Wagner, T., Pozzan, T., Pizzo, P., Scorrano, L., Brini, M., and Calì, T. (2018). SPLICS: a split green fluorescent protein-based contact site sensor for narrow and wide heterotypic organelle juxtaposition. Cell Death Differ. 25, 1131–1145.

Costa, R., Urbani, A., Salvalaio, M., Bellesso, S., Cieri, D., Zancan, I., Filocamo, M., Bonaldo, P., Szabò, I., Tomanin, R., and Moro, E. (2017). Perturbations in cell signaling elicit early cardiac defects in mucopolysaccharidosis type II. Hum. Mol. Genet. 26, 1643–1655.

Csordás, G., Várnai, P., Golenár, T., Roy, S., Purkins, G., Schneider, T.G., Balla, T., and Hajnóczky, G. (2010). Imaging interorganelle contacts and local calcium dynamics at the ER-mitochondrial interface. Mol. Cell 39, 121–132.

De Luca, A., Fiorillo, M., Peiris-Pagès, M., Ozsvari, B., Smith, D.L., Sanchez-Alvarez, R., Martinez-Outschoorn, U.E., Cappello, A.R., Pezzi, V., Lisanti, M.P., and Sotgia, F. (2015). Mitochondrial biogenesis is required for the anchorage-independent survival and propagation of stem-like cancer cells. Oncotarget 6, 14777–14795.

De Marchi, U., Castelbou, C., and Demaurex, N. (2011). Uncoupling protein 3 (UCP3) modulates the activity of Sarco/endoplasmic reticulum Ca2+-ATPase (SERCA) by decreasing mitochondrial ATP production. J. Biol. Chem. 286, 32533–32541.

Dupont, S., Morsut, L., Aragona, M., Enzo, E., Giulitti, S., Cordenonsi, M., Zanconato, F., Le Digabel, J., Forcato, M., Bicciato, S., et al. (2011). Role of YAP/TAZ in mechanotransduction. Nature 474, 179–183.

Enzo, E., Santinon, G., Pocaterra, A., Aragona, M., Bresolin, S., Forcato, M., Grifoni, D., Pession, A., Zanconato, F., Guzzo, G., et al. (2015). Aerobic glycolysis tunes YAP/TAZ transcriptional activity. EMBO J. 34, 1349–1370.

Fernandez-Vizarra, E., Bugiani, M., Goffrini, P., Carrara, F., Farina, L., Procopio, E., Donati, A., Uziel, G., Ferrero, I., and Zeviani, M. (2007). Impaired complex III assembly associated with BCS1L gene mutations in isolated mitochondrial encephalopathy. Hum. Mol. Genet. 16, 1241–1252.

Forkink, M., Basit, F., Teixeira, J., Swarts, H.G., Koopman, W.J.H., and Willems, P.H.G.M. (2015). Complex I and complex III inhibition specifically increase cytosolic hydrogen peroxide levels without inducing oxidative stress in HEK293 cells. Redox Biol. 6, 607–616.

Fulda, S., Galluzzi, L., and Kroemer, G. (2010). Targeting mitochondria for cancer therapy. Nat. Rev. Drug Discov. 9, 447–464.

Funato, Y., Michiue, T., Asashima, M., and Miki, H. (2006). The thioredoxin-related redox-regulating protein nucleoredoxin inhibits Wnt-beta-catenin signalling through dishevelled. Nat. Cell Biol. 8, 501–508.

Garcia, A.L., Udeh, A., Kalahasty, K., and Hackam, A.S. (2018). A growing field: the regulation of axonal regeneration by Wnt signaling. Neural Regen. Res. 13, 43–52.

Ghezzi, D., Arzuffi, P., Zordan, M., Da Re, C., Lamperti, C., Benna, C., D'Adamo, P., Diodato, D., Costa, R., Mariotti, C., et al. (2011). Mutations in TTC19 cause mitochondrial complex III deficiency and neurological impairment in humans and flies. Nat. Genet. 43, 259–263.

Giacomello, M., Drago, I., Bortolozzi, M., Scorzeto, M., Gianelle, A., Pizzo, P., and Pozzan, T. (2010). Ca2+ hot spots on the mitochondrial surface are generated by Ca2+ mobilization from stores, but not by activation of store-operated Ca2+ channels. Mol. Cell 38, 280–290.

Guzzo, G., Sciacovelli, M., Bernardi, P., and Rasola, A. (2014). Inhibition of succinate dehydrogenase by the mitochondrial chaperone TRAP1 has antioxidant and anti-apoptotic effects on tumor cells. Oncotarget 5, 11897–11908.

Ha, J., Daniel, S., Broyles, S.S., and Kim, K.H. (1994). Critical phosphorylation sites for acetyl-CoA carboxylase activity. J. Biol. Chem. 269, 22162–22168.

Herbst, A., Jurinovic, V., Krebs, S., Thieme, S.E., Blum, H., Göke, B., and Kolligs, F.T. (2014). Comprehensive analysis of β-catenin target genes in colorectal carcinoma cell lines with deregulated Wnt/β-catenin signaling. BMC Genomics 15, 74.

Homfray, T.F., Cottrell, S.E., Ilyas, M., Rowan, A., Talbot, I.C., Bodmer, W.F., and Tomlinson, I.P. (1998). Defects in mismatch repair occur after APC mutations in the pathogenesis of sporadic colorectal tumours. Hum. Mutat. 11, 114–120.

Horndasch, M., Lienkamp, S., Springer, E., Schmitt, A., Pavenstädt, H., Walz, G., and Gloy, J. (2006). The C/EBP homologous protein CHOP (GADD153) is an inhibitor of Wnt/TCF signals. Oncogene 25, 3397–3407.

Huang, X., Borgström, B., Stegmayr, J., Abassi, Y., Kruszyk, M., Leffler, H., Persson, L., Albinsson, S., Massoumi, R., Scheblykin, I.G., et al. (2018). The Molecular Basis for Inhibition of Stemlike Cancer Cells by Salinomycin. ACS Cent. Sci. 4, 760–767.

Ichimanda, M., Hijiya, N., Tsukamoto, Y., Uchida, T., Nakada, C., Akagi, T., Etoh, T., Iha, H., Inomata, M., Takekawa, M., and Moriyama, M. (2018). Down-regulation of dual-specificity phosphatase 4 enhances cell proliferation and invasiveness in colorectal carcinomas. Cancer Sci. 109, 250–258.

Ishii, I., Harada, Y., and Kasahara, T. (2012). Reprofiling a classical anthelmintic, pyrvinium pamoate, as an anti-cancer drug targeting mitochondrial respiration. Front. Oncol. 2, 137.

Jung, T.W., and Choi, K.M. (2016). Pharmacological Modulators of Endoplasmic Reticulum Stress in Metabolic Diseases. Int. J. Mol. Sci. 17, E192.

Kasahara, A., Cipolat, S., Chen, Y., Dorn, G.W., 2nd, and Scorrano, L. (2013). Mitochondrial fusion directs cardiomyocyte differentiation via calcineurin and Notch signaling. Science 342, 734–737.

Kishida, S., Yamamoto, H., Ikeda, S., Kishida, M., Sakamoto, I., Koyama, S., and Kikuchi, A. (1998). Axin, a negative regulator of the wnt signaling pathway, directly interacts with adenomatous polyposis coli and regulates the stabilization of beta-catenin. J. Biol. Chem. 273, 10823–10826.

Korinek, V., Barker, N., Morin, P.J., van Wichen, D., de Weger, R., Kinzler, K.W., Vogelstein, B., and Clevers, H. (1997). Constitutive transcriptional activation by a beta-catenin-Tcf complex in APC-/- colon carcinoma. Science 275, 1784–1787.

Kruspig, B., Valter, K., Skender, B., Zhivotovsky, B., and Gogvadze, V. (2016). Targeting succinate:ubiquinone reductase potentiates the efficacy of anti-cancer therapy. Biochim. Biophys. Acta 1863, 2065–2071.

Laskowski, M., Augustynek, B., Kulawiak, B., Koprowski, P., Bednarczyk, P., Jarmuszkiewicz, W., and Szewczyk, A. (2016). What do we not know about mitochondrial potassium channels? Biochim. Biophys. Acta 1857, 1247–1257.

Leanza, L., Romio, M., Becker, K.A., Azzolini, M., Trentin, L., Managò, A., Venturini, E., Zaccagnino, A., Mattarei, A., Carraretto, L., et al. (2017). Direct Pharmacological Targeting of a Mitochondrial Ion Channel Selectively Kills Tumor Cells In Vivo. Cancer Cell 31, 516–531.e10.

Lee, H.J., and Baek, S.S. (2017). Role of exercise on molecular mechanisms in the regulation of antidepressant effects. J. Exerc. Rehabil. 13, 617–620.

Lee, G., Goretsky, T., Managlia, E., Dirisina, R., Singh, A.P., Brown, J.B., May, R., Yang, G.Y., Ragheb, J.W., Evers, B.M., et al. (2010). Phosphoinositide 3-kinase signaling mediates beta-catenin activation in intestinal epithelial stem and progenitor cells in colitis. Gastroenterology 139, 869–881, 881.e1–881.e9.

Leem, Y.H., Kato, M., and Chang, H. (2018). Regular exercise and creatine supplementation prevent chronic mild stress-induced decrease in hippocampal neurogenesis via Wnt/GSK3β/β-catenin pathway. J. Exerc. Nutrition Biochem. 22, 1–6.

Li, N., Zhang, Y., Han, X., Liang, K., Wang, J., Feng, L., Wang, W., Songyang, Z., Lin, C., Yang, L., et al. (2015). Poly-ADP ribosylation of PTEN by tankyrases promotes PTEN degradation and tumor growth. Genes Dev. 29, 157–170.

Lu, D., and Carson, D.A. (2009). Spiperone enhances intracellular calcium level and inhibits the Wnt signaling pathway. BMC Pharmacol. 9, 13.

Lu, D., Choi, M.Y., Yu, J., Castro, J.E., Kipps, T.J., and Carson, D.A. (2011). Salinomycin inhibits Wnt signaling and selectively induces apoptosis in chronic lymphocytic leukemia cells. Proc. Natl. Acad. Sci. USA 108, 13253–13257.

Madreiter-Sokolowski, C.T., Gottschalk, B., Parichatikanond, W., Eroglu, E., Klec, C., Waldeck-Weiermair, M., Malli, R., and Graier, W.F. (2016). Resveratrol Specifically Kills Cancer Cells by a Devastating Increase in the Ca2+ Coupling Between the Greatly Tethered Endoplasmic Reticulum and Mitochondria. Cell. Physiol. Biochem. 39, 1404–1420.

Managò, A., Leanza, L., Carraretto, L., Sassi, N., Grancara, S., Quintana-Cabrera, R., Trimarco, V., Toninello, A., Scorrano, L., Trentin, L., et al. (2015). Early

effects of the antineoplastic agent salinomycin on mitochondrial function. Cell Death Dis. *6*, e1930.

Mills, E.L., Pierce, K.A., Jedrychowski, M.P., Garrity, R., Winther, S., Vidoni, S., Yoneshiro, T., Spinelli, J.B., Lu, G.Z., Kazak, L., et al. (2018). Accumulation of succinate controls activation of adipose tissue thermogenesis. Nature *560*, 102–106.

Montero, M., Brini, M., Marsault, R., Alvarez, J., Sitia, R., Pozzan, T., and Rizzuto, R. (1995). Monitoring dynamic changes in free Ca2+ concentration in the endoplasmic reticulum of intact cells. EMBO J. *14*, 5467–5475.

Moro, E., Ozhan-Kizil, G., Mongera, A., Beis, D., Wierzbicki, C., Young, R.M., Bournele, D., Domenichini, A., Valdivia, L.E., Lum, L., et al. (2012). In vivo Wnt signaling tracing through a transgenic biosensor fish reveals novel activity domains. Dev. Biol. *366*, 327–340.

Morris, S.L., and Huang, S. (2016). Crosstalk of the Wnt/β-catenin pathway with other pathways in cancer cells. Genes Dis. *3*, 41–47.

Morris, J.P., 4th, Wang, S.C., and Hebrok, M. (2010). KRAS, Hedgehog, Wnt and the twisted developmental biology of pancreatic ductal adenocarcinoma. Nat. Rev. Cancer *10*, 683–695.

Nicholls, D. (2013). Bioenergetics, 4th Edition (Academic Press).

Nusse, R., and Varmus, H.E. (1982). Many tumors induced by the mouse mammary tumor virus contain a provirus integrated in the same region of the host genome. Cell *31*, 99–109.

Ottolini, D., Calì, T., and Brini, M. (2014). Methods to measure intracellular Ca(2+) fluxes with organelle-targeted aequorin-based probes. Methods Enzymol. *543*, 21–45.

Pazini, F.L., Cunha, M.P., Azevedo, D., Rosa, J.M., Colla, A., de Oliveira, J., Ramos-Hryb, A.B., Brocardo, P.S., Gil-Mohapel, J., and Rodrigues, A.L.S. (2017). Creatine Prevents Corticosterone-Induced Reduction in Hippocampal Proliferation and Differentiation: Possible Implication for Its Antidepressant Effect. Mol. Neurobiol. *54*, 6245–6260.

Perez-Verdaguer, M., Capera, J., Serrano-Novillo, C., Estadella, I., Sastre, D., and Felipe, A. (2016). The voltage-gated potassium channel Kv1.3 is a promising multitherapeutic target against human pathologies. Expert Opin. Ther. Targets *20*, 577–591.

Ponce, A., Castillo, A., Hinojosa, L., Martinez-Rendon, J., and Cereijido, M. (2018). The expression of endogenous voltage-gated potassium channels in HEK293 cells is affected by culture conditions. Physiol. Rep. *6*, e13663.

Rasmussen, M.L., Ortolano, N.A., Romero-Morales, A.I., and Gama, V. (2018). Wnt Signaling and Its Impact on Mitochondrial and Cell Cycle Dynamics in Pluripotent Stem Cells. Genes (Basel) *9*, E109.

Ring, D.B., Johnson, K.W., Henriksen, E.J., Nuss, J.M., Goff, D., Kinnick, T.R., Ma, S.T., Reeder, J.W., Samuels, I., Slabiak, T., et al. (2003). Selective glycogen synthase kinase 3 inhibitors potentiate insulin activation of glucose transport and utilization in vitro and in vivo. Diabetes *52*, 588–595.

Rizzuto, R., De Stefani, D., Raffaello, A., and Mammucari, C. (2012). Mitochondria as sensors and regulators of calcium signalling. Nat. Rev. Mol. Cell Biol. *13*, 566–578.

Rozpedek, W., Pytel, D., Mucha, B., Leszczynska, H., Diehl, J.A., and Majsterek, I. (2016). The Role of the PERK/eIF2α/ATF4/CHOP Signaling Pathway in Tumor Progression During Endoplasmic Reticulum Stress. Curr. Mol. Med. *16*, 533–544.

Savignac, M., Simon, M., Edir, A., Guibbal, L., and Hovnanian, A. (2014). SERCA2 dysfunction in Darier disease causes endoplasmic reticulum stress and impaired cell-to-cell adhesion strength: rescue by Miglustat. J. Invest. Dermatol. *134*, 1961–1970.

Shen, M., Wang, L., Wang, B., Wang, T., Yang, G., Shen, L., Wang, T., Guo, X., Liu, Y., Xia, Y., et al. (2014). Activation of volume-sensitive outwardly rectifying chloride channel by ROS contributes to ER stress and cardiac contractile dysfunction: involvement of CHOP through Wnt. Cell Death Dis. *5*, e1528.

Shikata, Y., Kiga, M., Futamura, Y., Aono, H., Inoue, H., Kawada, M., Osada, H., and Imoto, M. (2017). Mitochondrial uncoupler exerts a synthetic lethal effect against β-catenin mutant tumor cells. Cancer Sci. *108*, 772–784.

Shimizu, N., Kawakami, K., and Ishitani, T. (2012). Visualization and exploration of Tcf/Lef function using a highly responsive Wnt/β-catenin signaling-reporter transgenic zebrafish. Dev. Biol. *370*, 71–85.

Shin, J., Park, H.C., Topczewska, J.M., Mawdsley, D.J., and Appel, B. (2003). Neural cell fate analysis in zebrafish using olig2 BAC transgenics. Methods Cell Sci. *25*, 7–14.

Szabo, I., and Zoratti, M. (2014). Mitochondrial channels: ion fluxes and more. Physiol. Rev. *94*, 519–608.

Traver, D., Paw, B.H., Poss, K.D., Penberthy, W.T., Lin, S., and Zon, L.I. (2003). Transplantation and in vivo imaging of multilineage engraftment in zebrafish bloodless mutants. Nat. Immunol. *4*, 1238–1246.

van Lidth de Jeude, J.F., Meijer, B.J., Wielenga, M.C.B., Spaan, C.N., Baan, B., Rosekrans, S.L., Meisner, S., Shen, Y.H., Lee, A.S., Paton, J.C., et al. (2017). Induction of endoplasmic reticulum stress by deletion of Grp78 depletes Apc mutant intestinal epithelial stem cells. Oncogene *36*, 3397–3405.

Verras, M., Papandreou, I., Lim, A.L., and Denko, N.C. (2008). Tumor hypoxia blocks Wnt processing and secretion through the induction of endoplasmic reticulum stress. Mol. Cell. Biol. *28*, 7212–7224.

Viale, A., Pettazzoni, P., Lyssiotis, C.A., Ying, H., Sánchez, N., Marchesini, M., Carugo, A., Green, T., Seth, S., Giuliani, V., et al. (2014). Oncogene ablation-resistant pancreatic cancer cells depend on mitochondrial function. Nature *514*, 628–632.

Wek, R.C., Jiang, H.Y., and Anthony, T.G. (2006). Coping with stress: eIF2 kinases and translational control. Biochem. Soc. Trans. *34*, 7–11.

Wen, Y.A., Xiong, X., Scott, T., Li, A.T., Wang, C., Weiss, H.L., Tan, L., Bradford, E., Fan, T.W.M., Chandel, N.S., et al. (2019). The mitochondrial retrograde signaling regulates Wnt signaling to promote tumorigenesis in colon cancer. Cell Death Differ. Published online January 18, 2019. https://doi.org/10.1038/s41418-018-0265-6.

Yoon, J.C., Ng, A., Kim, B.H., Bianco, A., Xavier, R.J., and Elledge, S.J. (2010). Wnt signaling regulates mitochondrial physiology and insulin sensitivity. Genes Dev. *24*, 1507–1518.

Yung, H.W., Charnock-Jones, D.S., and Burton, G.J. (2011). Regulation of AKT phosphorylation at Ser473 and Thr308 by endoplasmic reticulum stress modulates substrate specificity in a severity dependent manner. PLoS One *6*, e17894.

Zhang, L.S., and Lum, L. (2018). Chemical Modulation of WNT Signaling in Cancer. Prog. Mol. Biol. Transl. Sci. *153*, 245–269.

Zhang, X., Mofers, A., Hydbring, P., Olofsson, M.H., Guo, J., Linder, S., and D'Arcy, P. (2017). MYC is downregulated by a mitochondrial checkpoint mechanism. Oncotarget *8*, 90225–90237.

STAR★METHODS

KEY RESOURCES TABLE

REAGENT or RESOURCE	SOURCE	IDENTIFIER
Antibodies		
β-catenin	Sigma-Aldrich	Cat#C7082; RRID:AB_258995
β-catenin pS552	Cell Signaling Technology	Cat#9566
MET	Cell Signaling Technology	Cat#8198; RRID:AB_10858224
LEF1	Cell Signaling Technology	Cat#2230; RRID:AB_823558
CD44	Cell Signaling Technology	Cat#3570; RRID:AB_2076465
GSK3α/β	Cell Signaling Technology	Cat#5676; RRID:AB_10547140
GSK3α/β pS21/9	Cell Signaling Technology	Cat#8566; RRID:AB_10860069
Wnt5a/b	Cell Signaling Technology	Cat#2530; RRID:AB_2215595
NFATc1	Santa Cruz Biotechnologies	Cat#sc-7294; RRID:AB_2152505
Akt	Cell Signaling Technology	Cat#9272; RRID:AB_329827
Akt pS473	Cell Signaling Technology	Cat#4060; RRID:AB_2224726
ACC pS79	Santa Cruz Biotechnologies	Cat#sc-271965; RRID:AB_1526014
Bip (GRP78)	Cell Signaling Technology	Cat#3183; RRID:AB_10695864
eIF2α pS51	Abcam	Cat#ab32157; RRID:AB_732117
eIF2α	Abcam	Cat#ab5369; RRID:AB_304838
ATF4	Santa Cruz Biotechnologies	Cat#sc-200; RRID:N.D.
GAPDH	Millipore	Cat#CB1001; RRID:AB_2107426
β-actin	Millipore	Cat#MAB1501; RRID:AB_2223041
TCF7	Sigma-Aldrich	Cat#WH0006932M1; RRID:AB_1843894
MFN2	Abnova	Cat#H00009927-M03; RRID:AB_530127
SERCA	Thermo Fisher Scientific	Cat#MA3-910; RRID:AB_2227681
Calnexin	Stressgen	Cat#SPA-860; RRID:AB_2069021
Calreticulin	Stressgen	Cat#SPA-601; RRID:AB_2038900
Anti-mouse secondary antibody	Sigma-Aldrich	Cat#A4416; RRID:AB_258167
Anti-rabbit secondary antibody	KPL	Cat#074-1516; RRID:N.D.
Chemicals, Peptides, and Recombinant Proteins		
Cyclosporine H	Sequoia	Cat#SRP046746c
PAP-1	Sigma Aldrich	Cat#P6124
Staurosporine	Sigma Aldrich	Cat#S4400
CHIR99021	Sigma Aldrich	Cat#SML1046
XAV939	Sigma Aldrich	Cat#X3004
Cyclopamine	Sigma Aldrich	Cat#C4116
Valinomycin	Sigma Aldrich	Cat#V0627
Salinomycin	Sigma Aldrich	Cat#S4526
Nigericin	Sigma Aldrich	Cat#N7143
Rotenone	Sigma Aldrich	Cat#R8875
2-Thenoyltrifluoroacetone (TTFA)	Sigma Aldrich	Cat#T27006
Antimycin A	Sigma Aldrich	Cat#A8674
Oligomycin	Sigma Aldrich	Cat#75351
carbonyl cyanide-4-(trifluoromethoxy)phenylhydrazone (FCCP)	Sigma Aldrich	Cat#C2920
Atractyloside	Sigma Aldrich	Cat#A6882
Thapsigargin	Sigma Aldrich	Cat#T9033
Tunicamycin	Sigma Aldrich	Cat#T7765

(Continued on next page)

Continued

REAGENT or RESOURCE	SOURCE	IDENTIFIER
Creatine	Sigma Aldrich	Cat#C3630
Phosphoenolpyruvate	Sigma Aldrich	Cat#860077
4-phenylbutirric acid (4-PBA)	Sigma Aldrich	Cat#SML0309
Margatoxin (MgTx)	Alomone Lab	Cat#STM-325
Charybdotoxin (ChTx)	Alomone Lab	Cat#STC-325
Stichodactylatoxin (ShK)	Alomone Lab	Cat#STS-400
PAPTP	Leanza et al., 2017	N/A
PCARBTP	Leanza et al., 2017	N/A
DMSO	Sigma Aldrich	Cat#D2650
TRIzoL	Thermo Fisher Scientific	Cat#15596026
D-Luciferin	Sigma Aldrich	Cat#L9504
Chlorophenolred-β-D-galactopyranoside (CPRG)	Roche	Cat#10884308001
2-deoxy-D-glucose	Sigma Aldrich	Cat#D8375
TransIT®-LT1 transfectionreagent	Mirus	Cat#MIR2304
Coelenterazine	Santa Cruz Biotechnologies	Cat#sc-205904
Ionomycin	Sigma Aldrich	Cat#I3909
Critical Commercial Assays		
CellTiter 96® AQUEOUS One solution	Promega	Cat#G3581
Superscript reverse transcriptase kit	Thermo Fisher Scientific	Cat#12594025
ATP Lite luminescence ATP detection assay system	Perkin Elmer	Cat#6016947
Power SYBR Green PCR master mix	Thermo Fisher Scientific	Cat#4367659
Experimental Models: Cell Lines		
Human: HEK293	ATCC	CRL-1573
Human: DLD1	ATCC	CCL-221
Human: HCT116	ATCC	CCL-247
Human: HeLa	ATCC	CCL-2
Human immortalized fibroblasts *bcs1l*$^{wt/wt}$	Fernandez-Vizarra et al., 2007	N/A
Human immortalized fibroblasts *bcs1l*$^{R73C/F368I}$	Fernandez-Vizarra et al., 2007	N/A
Experimental Models: Organisms/Strains		
Zebrafish: Tg(7xTCFX.lasiam:mCherry)ia5	Moro et al., 2012	ZFIN: ZDB-alt-110113-2
Zebrafish: Tg(7xTCFX.lasiam:GFP)ia4	Moro et al., 2012	ZFIN: ZDB-alt-110113-1
Zebrafish: Tg(12xGli.HSV:GFP)ia11	Costa et al., 2017	ZFIN: ZDB-alt-120404-2
Zebrafish: Tg(Olig2:gfp)vu12	Shin et al., 2003	ZFIN: ZDB-alt-041129-8
Zebrafish: Tg(Gata1:dsred)sd2	Traver et al., 2003	ZFIN: ZBD-alt-051223-6
Oligonucleotides		
hGAPDH (for): CACAATATCACTTTACCAGAGTTAAAAGC	This paper	N/A
hGAPDH (rev): CGAGCCACATCGCTCAGAC	This paper	N/A
hβ-catenin (for): CGAATGTCTGAGGACAAGCCACA	This paper	N/A
hβ-catenin (rev): CCATATCCACCAGAGTGAAAAGA	This paper	N/A
hCyclin D1 (for): GGGGAGGAGAACAAACAGAT	This paper	N/A
hCyclin D1 (rev): TGAGGCGGTAGTAGGACAGG	This paper	N/A
hDKK1 (for): CAGGCGTGCAAATCTGTCT	This paper	N/A
hDKK1 (rev): CCCATCCAAGGTGCTATGAT	This paper	N/A
hAxin1 (for): ACAGGATCCGTAAGCAGCAC	This paper	N/A
hAxin1 (rev): GCTCCTCCAGCTTCTCCTC	This paper	N/A
Recombinant DNA		
M50 Super 8x TOPFlash	Addgene	Cat#12456
RBPJ-lux	Gift from Prof. C. Kintner	N/A

REAGENT or RESOURCE	SOURCE	IDENTIFIER
8xGTIIC-luciferase	Addgene	Cat#34615
F-XBP1ΔDBD	Gift from Prof. T. Iwawaki	N/A
CMV-lux	Gift from Prof. A. Rosato	N/A
CMV-β-gal	Azzolin et al., 2012	N/A
stable β-catenin expressing vector	Azzolin et al., 2012	N/A
pRK5-mWnt3a	Addgene	Cat#42277
pBlueScript II SK (+)	Addgene	Cat#212205
NΔE	Gift from Prof. C. Kintner	N/A
aequorin construct targeted to the ER (erAEQ)	Ottolini et al., 2014	N/A
MFN2-overexpressing plasmid	Cieri et al., 2018	N/A
Software and Algorithms		
Image Lab	BioRad Laboratories	N/A
Prism 6.0	Graph Pad	N/A
GIMP 2.0	https://www.gimp.org	N/A
iQiCycler	BioRad Laboratories	N/A
O$_2$ View	Hansatech Instruments	N/A

LEAD CONTACT AND MATERIALS AVAILABILITY

Further information and requests for reagents may be directed to and will be fulfilled by the corresponding author Luigi Leanza (luigi.leanza@unipd.it).

This study did not generate new unique reagents.

EXPERIMENTAL MODEL AND SUBJECT DETAILS

Animal studies

Zebrafish (animals and embryos) were maintained according to standard rules and procedures (https://zfin.org). All animal manipulation procedures were conducted according to the Local Ethical Committee at the University of Padua and National Agency (Italian Ministry of Health Authorization number 407/2015-PR), and with the supervision of the Central Veterinary Service of the University of Padova (in compliance with Italian Law DL 116/92 and further modifications, embodying UE directive 86/609).

Cell cultures

In vitro experiments were performed with HEK293, HeLa, HCT116 and DLD1 cells. HEK293, HeLa and HCT116 cells were cultured in Dulbecco's modified Eagle medium (DMEM, Invitrogen), supplemented with 10% fetal bovine serum (FBS, BioSpa S.p.A.), 10 mM HEPES (Life Techologies), 100 U/ml penicillin and 100 U/ml streptomycin (Life Technologies), 1X non-essential amino acids (Life Technologies). DLD1 cells were cultured in Roswell Park Memorial Institute (RPMI) 1640 medium (Invitrogen), supplemented with 10% fetal bovine serum (FBS, BioSpa S.p.A.), 10 mM HEPES (Life Techologies), 100 U/ml penicillin and 100 U/ml streptomycin (Life Technologies), 1X non-essential amino acids (Life Technologies). All cells were maintained at 37°C and 5% CO$_2$. Furthermore, we used human immortalized fibroblasts obtained from healthy human subjects harboring a gene codifying the respiratory chain complex III assembly factor *bcs1l*$^{wt/wt}$ (wt) or from a patient with deficiency of the respiratory chain complex III, due to a *bcl1s* composed heterozygosis (*bcs1l*$^{R73C/F368l}$) (Fernandez-Vizarra et al., 2007). These human cells were maintained in culture in DMEM supplemented as stated above.

METHOD DETAILS

Reagents

The following compounds were obtained from Sigma-Aldrich: CHIR99021 and XAV939, two Wnt signaling modulators; cyclopamine, an inhibitor of the Sonic-Hedgehog pathway; DAPT, a Notch inhibitor; Forskolin and 3-isobutyl-1-methyl-xanthine (IBMX), used to block Hippo pathway; valinomycin, a potassium ionophore; salinomycin and nigericin, two potassium antiporters; rotenone, 2-Thenoyltrifluoroacetone (TTFA), antimycin A, oligomycin, the respiratory chain complexes inhibitors; the mitochondrial uncoupler FCCP (Carbonyl cyanide-p-trifluoromethoxyphenylhydrazone); atractyloside, a blocker of the mitochondrial adenine nucleotide transporter (ANT); the SERCA inhibitor thapsigargin; tunicamycin, an inducer of the unfolding protein response (UPR); Creatine and phosphoenolpyruvate, to stimulate cellular ATP production; 4-phenylbutirric acid (4-PBA), an inhibitor of ER stress; staurosporine, an inducer of the intrinsic

apoptotic pathway, PAP-1, a membrane permeant inhibitor of the potassium channel Kv1.3. Margatoxin (MgTx), Stichodactyla toxin (ShK) and Charybdotoxin (ChTx) were from Alomone Lab. The mitochondria-targeted Kv1.3 inhibitors (3-(4-(4-((7-oxo-7H-furo[3,2-g]benzopyran-4-yl)oxy)butoxy)phenyl)propyl)triphenyl phosphonium iodide (PAPTP) and (3-(((4-(4-((7-oxo-7H-furo[3,2-g]benzopyran-4-yl)oxy)butoxy)phenoxy)carbonyl) amino) propyl) triphenylphosphonium iodide (PCARBTP) were synthesized as described previously (Leanza et al., 2017). All compounds were dissolved in DMSO. In HEK293 cells, Wnt signaling is not active, thus it was induced with CHIR99021, a well-established Wnt signaling activator that acts by inhibiting GSK3β activity (Ring et al., 2003), hence favoring β-catenin stabilization, or by transfection with a plasmid expressing the Wnt3A ligand. Consequently, cells treated with 0.2% DMSO were used as a negative control and cells treated with 3 μM CHIR99021 were considered the positive control.

Protein lysates and electrophoresis

Total protein extracts were obtained from cells. After removing the culture medium, cells were washed twice in ice-cold phosphate buffer saline (PBS), detached and resuspended in 1.5 mL of PBS and transferred into a 2 mL Eppendorf tube. After 5 minutes of centrifugation at 1,200 g, the pellet was resuspended in 600 μL of ice-cold lysis buffer (0.3X PBS, 0.5% Triton X-100, 0.5% Sodium Dodecyl Sulfate), vortexed for 20 s and then centrifuged at 20000 g for 20 minutes at 4°C. The supernatant, containing proteins, was transferred to a new eppendorf tube and stored at −80°C until use. Proteins were separated by sodium dodecyl sulfate polyacrylamide gel electrophoresis (SDS-PAGE). All gels used were NuPage 4%–12% Bis-Tris protein gels from ThermoFisher Scientific using NuPage MES as running buffer (Thermofisher Scientific). Protein lysates were pre-incubated with Laemmli sample buffer and loaded into the wells. PageRuler Plus Prestained Protein Ladder (Thermofisher Scientific) was loaded in the first lane as molecular weight standard.

Western Blotting

Western Blot was performed with PVDF membranes. 50 μg of protein were loaded in each lane of 4%–12% NuPage Bis-Tris precast gels (Thermo Fisher Scientific – NP0321BOX). The transfer was performed with NuPage Transfer Buffer. Membranes were blocked in skim milk (Sigma-Aldrich, 5% in Tris-buffered saline (TBS: 10 mM Tris, 150 mM NaCl, pH 7.4) for 2 hours at RT and washed in TBS. Membranes were incubated overnight at 4°C with the following primary antibodies all diluted in TBS-Tween (TTBS: TBS + 0.05% Tween (Sigma-Aldrich) 20%): β-catenin (1:2000 - Sigma-Aldrich C7082); β-catenin pS552 (1:1000 - CST #9566); MET (1:1000 - CST #8198); LEF1 (1:500 - CST #2230); CD44 (1:1500 - CST #3570); GSK3α/β (1:1000 - CST #5676); GSK3α/β pS21/9 (1:1000 - CST #8566); Wnt5a/b (1:1500 - CST #2530); NFATc1 (1:1000 - SCBT sc-7294); Akt (1:1000 - CST #9272); Akt pS473 (1:1000 - CST #4060); ACC pS79 (1:500 - SCBT sc-271965); BiP (GRP78 – 1:1000 - CST #3183); eIF2α pS51 (1:1000 - Abcam ab32157); eIF2α (1:1000 – Abcam ab5369); ATF4 (1:500 - SCBT sc-200); TCF7 (1:1000 – Sigma-Aldrich WH0006932M1); GAPDH (1:1000 - EMD Millipore CB1001); β-actin (1:3000 - EMD Millipore MAB1501); MFN2 (1:1000 – abnova H00009927-M03); SERCA (1:2000 - Thermo Fisher Scientific MA3-910); Calnexin (1:5000 – Stressgen SPA-860); Calreticulin (1:2000 – Stressgen SPA-601). Anti-mouse or anti-rabbit secondary antibodies conjugated to horseradish peroxidase (HRP; dilution 1:10000 in TTBS; mouse: Sigma-Aldrich A4416; rabbit: KPL 074-1516) were used for protein detection. Chemiluminescence was detected with ChemiDoc Touch Imaging System (BioRad) after incubation with EuroCloneLiteAblot Plus luminol mix. Densitometric analyses were performed with Image Lab Software (BioRad). β-actin or GAPDH were used as loading controls. Statistical analyses were performed with GraphPad Prism 5.

Real-Time PCR

RNA extraction was performed with TRIzol (Thermofisher Scientific), following the manufacturer's protocol. Total RNA was quantified with NanoDrop 2000 Spectrophotometer (Thermofisher Scientific). SuperScript II Reverse Transcriptase kit (ThermoFisher Scientific) was used for retrotranscription, as indicated by the supplier, using Mastercycler (Eppendorf). The synthetized cDNA was subjected to RT-PCR with Power SYBR® Green PCR Master Mix (ThermoFisher Scientific) following supplier's instructions. iQiCycler (BioRad) was used for the amplification reaction and plate reading. *Gapdh* was used as housekeeping gene for normalization.
Primers for RT-PCR

Target	Sequence (from 5' to 3')	Accession number
hGAPDH (for)	CACAATATCACTTTACCAGAGTTAAAAGC	NM_002046.5
hGAPDH (rev)	CGAGCCACATCGCTCAGAC	NM_002046.5
hβ-catenin (for)	CGAATGTCTGAGGACAAGCCACA	NM_001904.3
hβ-catenin (rev)	CCATATCCACCAGAGTGAAAAGA	NM_001904.3
hCyclin D1 (for)	GGGGAGGAGAACAAACAGAT	NM_053056.2
hCyclin D1 (rev)	TGAGGCGGTAGTAGGACAGG	NM_053056.2
hDKK1 (for)	CAGGCGTGCAAATCTGTCT	NM_012242.2
hDKK1 (rev)	CCCATCCAAGGTGCTATGAT	NM_012242.2
hAxin1 (for)	ACAGGATCCGTAAGCAGCAC	NM_003502.3
hAxin1 (rev)	GCTCCTCCAGCTTCTCCTC	NM_003502.3

MTS assay

To measure viability of the cells, HEK293, HCT116 and DLD1 cells were seeded into 96-well plates at a density of 20×10^3 cells/well. After 24 hours, the growth medium was replaced with phenol red- and FBS-free medium and treated with the drugs: four wells were used for each condition. After 8 or 24 hours of incubation with different drugs 10% CellTiter 96® AQUEOUS One solution (Promega, Italy) was added to each well. Finally, absorbance at 490 nm was measured using an Infinite® 200 PRO 96-well plate reader. Since the assay is based on dehydrogenase activity, that is inhibited by TTFA (Guzzo et al., 2014), the MTT absorbance is lower in the presence of the drug. We therefore controlled by addition of FITC-labeled annexin V that cells after TTFA treatment were not dead (not shown).

Luciferase assays

Luciferase assays were performed in HEK293, HCT116 and DLD1 cell lines. Cells were transfected with one of the following plasmids: β-catenin/TCF-responsive reporter TOP-FLASH (M50 Super 8x TOPFlash, Addgene, Cat#12456), YAP/TAZ-responsive reporter 8xGTIIC-Lux (Addgene, Cat#34615), Notch-responsive reporter RBPJ-Lux (a gift from Prof. C. Kintner), ER-stress responsive reporter F-XBP1ΔDBD (a gift from Prof. T. Iwawaki). Transfection performed with CMV-Lux (a gift from Prof. A. Rosato) reporter was used as control. To induce Wnt signaling in some experiments, cells were transfected together with stable β-catenin expressing vector (Azzolin et al., 2012) or Wnt3a expressing construct (pRK5-mWnt3a, Addgene, Cat#42277). To induce Notch signaling, co-transfection with NΔE (a gift from Prof. C. Kintner) was performed. Luciferase reporters were transfected together with CMV-β-gal (Azzolin et al., 2012) to normalize for transfection efficiency with CPRG (Roche). DNA content was kept uniform by using pBlueScript II SK (Addgene, Cat#212205).

Cells were plated in 24-well plates at a density of 5×10^4 cells/well. After 24 hours luciferase reporter plasmids were transiently transfected using TransIT®-LT1 Transfection Reagent (Mirus). 48 hours after transfection, cells were treated with different compounds for 8 hours and then harvested in Luc lysis buffer (25 mM Tris pH 7.8, 2.5 mM EDTA, 10% glycerol, 1% NP-40, 2 mM DTT). Luciferase activity was determined in a Tecan plate luminometer with freshly reconstituted assay reagent (0.5 mM D-Luciferin, 20 mM tricine, 1 mM $(MgCO_3)$-4$Mg(OH)_2$, 2.7 mM $MgSO_4$, 0.1 mM EDTA, 33 mM DTT, 0.27 mM CoA, 0.53 mM ATP).

The luciferase signal was normalized with respect to the β-gal signal that was used to co-transfect the cells, as normalization of the luciferase signal with respect to the cell number would not take into consideration that not all cells are transfected. Thus, the measured luciferase signal refers only to the transfected and living cells (otherwise β-gal would not be expressed) as previously described (Azzolin et al., 2014; Dupont et al., 2011).

Determination of ATP concentration

ATP amount was measured in HEK293, in HCT116, in DLD1 and in human immortalized fibroblasts, using ATPlite Luminescence ATP Detection Assay System (Perkin Elmer). Cells were seeded into white 96-well viewplates at a density of 4×10^4 cells/well for HEK293 and HCT116, 3×10^4 cells/well for DLD1 and 1.5×10^4 cells/well for human immortalized fibroblasts. To measure mitochondrial ATP production, 24 hours after seeding glycolysis was inhibited pre-incubating cells with 5.5 mM 2-deoxy-D-glucose (2-DG) for 1 h and then all treatments were performed in medium containing 2-DG. Oligomycin was used as positive control. 6 hours after treatments, the assay was performed according to manufacturer's instructions.

In vivo experiments

WT zebrafish were from the Tübingen (Tü) or AB strains. All transgenic lines were collected from original laboratories which developed the lines and are currently stabled at the zebrafish facility of University. All transgenic lines were previously reported, Sonic-Hedgehog (Shh) reporter Tg(12xGli.HSV:GFP)[ia11] (ZFIN: ZDB-alt-120404-2), Tg(Olig2:gfp)[vu12] (ZFIN: ZDB-alt-041129-8) (Moro et al., 2012), Tg(Gata1:dsred)[sd2] (ZFIN: ZBD-alt-051223-6) (Shin et al., 2003). Tg(7xTCFX.lasiam:EGFP)[ia4] contains a *gfp* gene driven by a *tcf./lef* responding promoter. This line reports Wnt signaling activity *in vivo*. Tg(Olig2:GFP)[vu12] contains *gfp* gene under control of a fragment derived from the oligodendrocyte transcription factor 2 (Olig2) promoter region, this line accounts for olig2 transcription *in vivo* (Traver et al., 2003). Tg(gata1:dsRed)[sd2] transgene contains the dsRed cDNA under control of a 7-kb fragment derived from the gata1 promoter (Traver et al., 2003). This line reports all erythroid lineages (Gata1+) *in vivo*.

Zebrafish embryos expressing fluorescent proteins were analyzed using a Leica M165FC epifluorescent microscope. All images were acquired with a Nikon DS-F12 digital camera. All images were acquired with the same exposure parameters and processed *in silico* with GIMP 2.0. Western blot experiments, fish larvae were lysed in buffer (50 mM Tris pH 7.5, 150 mM NaCl, 0.02% NP-40 supplemented with protease inhibitor (Roche Diagnostics) and Phosphatase Inhibitor Cocktails 2 and 3 (Sigma-Aldrich). Sample homogenization was performed with a glass dounce. The lysates were centrifuged at 13000 g for 30 min at 4°C. Supernatants were analyzed by SDS-PAGE/WB as described above.

Morpholinos injection, Oxygraph analysis and rescue

Custom Morpholinos were purchased by Genetools LLC. Bcs1l spMO (5′-AGCACAACAGCAAGACATACTCTCG-3′) affects splicing donor site of the exon 5 in *D. rerio* bcs1l mRNA(-). Ttc19 spMO (5′-AAGGCTGATGTGAAAGCAAATCTGA-3′) affects exon 2 splicing acceptor site in *D. rerio* ttc19 mRNA. Standard Ctrl Morpholino (Ctrl MO) was purchased by Genetools LLC. Microinjection is performed on randomly separated sibling embryos at 1 cell stage, adding ≈30ng/embryos of morpholino. Chorions were manually

excided at 24hpf and images were acquired at 48hpf, crude proteins extract were also obtained after images acquisition (See section above). Respiratory deficiency was assessed by Oxygraph+ (Hansatech instruments), O_2 concentration in the media and O_2 consumption were revealed by O_2 view software. 15 randomly selected embryos were displayed in the sample chamber (2ml fish water, 28°C, 50rpm), recording started after a stabilization period of 180 s, acquisition was performed for 780 s. Pictures report 300 s of a single experiment with Ctrl MO; Bcs1l spMO; Ttc19 spMO, 3 independent experiments were performed for each condition. O_2 concentration in the media and O_2 consumption reported in graphs show pooled data from three independent experiments and paired t test has been performed (* = p < 0.05). Recovery experiments were performed by the co-injection in siblings' embryos at 1 cell stage of 650 ng/larva of Creatine (Sigma Aldrich) and 30 ng/larva of splicing morpholino. Pictures acquisition were performed at 48hpf by Leica M165FC epifluorescent microscope. A single embryo representative of 3 different independent experiments was reported in each picture.

ER-mitochondria Contact Site Analysis

Cells plated on 13-mm-diameter coverslips were transfected with SPLICS$_S$ (Cieri et al., 2018) together with empty or MFN2 expressing vector. We have previously developed this splitGFP and BICF-based probe to specifically monitor ER-mitochondria contacts in the range of 8-10 nm (Cieri et al., 2018), i.e., those that are occurring at the distance range suitable to modulate ER-mitochondria Ca^{2+} transfer ((Csordás et al., 2010; Giacomello et al., 2010). Fluorescence was analyzed in living cells by a Leica SP5 confocal microscope. Cells were excited at 488 nm and confocal stacks were acquired every 0.2 μm along the z axis with a 63 × objective. For mitochondria-ER interaction analysis, stacks were automatically analyzed using ImageJ, deconvoluted, three-dimensional-reconstructed, and surface-rendered by using VolumeJ (ImageJ). Interactions were quantified as already described (Cieri et al., 2018).

Calcium uptake measurements

HEK293 or HeLa cells were seeded onto 6-well plates 12 h before transfection and allowed to grow to 60%–80% confluence. Transfection was carried out with the Ca^{2+}-phosphate procedure, using 12 μg for each well of the 6-well plate. For Ca^{2+} measurement cells were co-transfected with low affinity aequorin construct targeted to the ER (erAEQ) alone or together with MFN2-overexpressing vector (Ottolini et al., 2014). Twenty-four hours after transfection, cells were plated onto a 96-well plate. The day after, HEK293 cells were incubated for 8 hours with the different drugs before Ca^{2+} measurements. Ca^{2+} concentration measurements were carried out in a Perkin-Elmer Envision plate reader equipped with a two-injectors unit.

To measure steady state Ca^{2+} levels in the lumen of the ER, transfected aequorin needs to be reconstituted in its active form by adding the prosthetic group coelenterazine. Considering the high amount of Ca^{2+} in the ER lumen, to obtain sufficient amount of reconstituted aequorin and to avoid the consumption before starting the measurements, it is necessary to drastically reduce ER Ca^{2+} content. Thus, the cells were incubated for 1.5 h at 4°C in modified Krebs Ringer Buffer (KRB: 125 mM NaCl, 5 mM KCl, 400 mM KH_2PO_4, 1 mM $MgSO_4$, 20 mM HEPES, pH 7.4) supplemented with 5 mM glucose, 5 μM of the Ca^{2+} ionophore ionomycin (Sigma), 600 μM EGTA and 5 μM of the hydrophobic prosthetic group coelenterazine n (Santa Cruz Biotechnology). Cells were then extensively washed with KRB supplemented with 2% bovine serum albumin (Sigma) and 1 mM EGTA to remove ionomycin and were placed in 70 μL of KRB supplemented with 5 mM glucose and 75 μM EGTA and luminescence from each well was measured. After 10 s, 1 mM $CaCl_2$ at the final concentration was injected to refill the ER lumen. After Ca^{2+} re-addition, a plateau was reached in about two minutes and its level, reported upon calibration of photons emission in Ca^{2+} concentration values was indicative of the steady state Ca^{2+} level in the ER. To calibrate photons emission in Ca^{2+} concentration values, the total amount of active aequorin in each coverslip needs to be discharged (Brini et al., 1995). Thus, the experiments were terminated by lysing the cells with 100 μM digitonin (Sigma) in a hypotonic Ca^{2+}-rich solution (10 mM $CaCl_2$ in H_2O) to consume the remaining reconstituted aequorin pool. Output data were analyzed and calibrated with a custom made macro-enabled Excel workbook as previously described (22).

QUANTIFICATION AND STATISTICAL ANALYSIS

Statistically significant difference was assessed for each treatment by means of one-way ANOVA analysis with Dunnett's post test. All statistical analyses were performed using GraphPad Prism software. Statistical details can be found in all figure legends.

DATA AND CODE AVAILABILITY

This study did not generate/analyze datasets/code.

Supplemental Information

Impaired Mitochondrial ATP

Production Downregulates Wnt

Signaling via ER Stress Induction

Roberto Costa, Roberta Peruzzo, Magdalena Bachmann, Giulia Dalla Montà, Mattia Vicario, Giulia Santinon, Andrea Mattarei, Enrico Moro, Rubén Quintana-Cabrera, Luca Scorrano, Massimo Zeviani, Francesca Vallese, Mario Zoratti, Cristina Paradisi, Francesco Argenton, Marisa Brini, Tito Calì, Sirio Dupont, Ildikò Szabò, and Luigi Leanza

Supplementary Material

Supplementary Figure legends.

Figure S1. Mitochondrial fitness does not affect other signaling pathways *in vitro* and *in vivo*. Related to Figure 1. (A) A representative Western blot showing protein levels of β-catenin after 8 hours treatment with 0.1% DMSO (used as negative control), 1µM PAPTP with (+) or without (-) 3 µM CHIR. 50 µg of protein extract from HEK293 cells were loaded. β-actin was used as loading control. **(B)** Viability of HEK293 cells was assayed after 8 hours of treatment with MTS assays, to confirm sub-lethal dosage of the compounds after the 8 hours-treatment used throughout the study. Cells were treated with the following compounds: 0.1% DMSO, as negative control; 10% DMSO as positive controls; 3 µM CHIR99021 (CHIR); 10 µM XAV939 (XAV); 1 µM PAPTP and 5 µM PCARBTP, mitochondrial Kv1.3 inhibitors; potassium fluxes modulators, 5 µM salinomycin (Salino), 1 µM valinomycin (Valino), 0.5 µM nigericin (Nige); 2 µM of the uncoupler FCCP; respiratory chain complexes inhibitors, 5 µM rotenone (Rot), 0.5 mM TTFA, 10 µg/ml antimycin A (Anti), 1 µg/ml oligomycin (Oligo); 1 µM SERCA inhibitor thapsigargin (Thapsi) and 0.5 µg/ml UPR-inducer tunicamycin (Tunica); 10 µM of the adenine nucleotide transporter (ANT) blocker atractyloside (Atracty). The values are reported as means of percentages +/- SEM of MTS absorbance measured at 490 nm related to DMSO-treated samples, indicated in the graph as "*ref*" (n=3). **(C)** To verify that the decrease in luciferase signal was not directly due to inhibition of enzymatic activity upon treatment with the different drugs but was dependent on the modulation of a signaling pathway, HEK293 cells were transfected with a plasmid encoding a luciferase under the control of the CMV promoter. Then cells were treated for 8 hours as in S1B. The values are reported as means of percentages of luciferase signal +/- SEM related to DMSO treated sample, indicated in the graph as "*ref*" (n=3). **(D-E)** Canonical Wnt signaling activity based on TCF/LEF dependent transcription was assayed in HEK293 cells, which were transfected with a TOP-FLASH plasmid codifying a luciferase reporter gene under the control of a TCF/LEF promoter. In these cells we either induced or not the Wnt signaling by co-transfection with stable β-catenin- (D) or Wnt3A-expressing (E) plasmids. Furthermore, HEK293 cells were treated for 8 hours with the compounds as in S1B. The values are reported as percentage of luciferase signal related to the induced control indicated in the graph as "*ref*". Values are means +/- SEM (n=3). **(F-G)** The specificity for the mito-Wnt axis was further demonstrated by the *in vitro* study of other two signaling pathways, namely Notch (F) and Hippo (G). The Notch signaling was assayed by co-transfecting HEK293 cells with both a RBPJ-lux plasmid codifying luciferase under the control of a Notch-dependent promoter and the NΔE plasmid to induce this signaling pathway. Conversely, the Hippo pathway activity was measured by transfecting cells with the 8xGTIIC luciferase reporter plasmid. As positive controls, DAPT for the Notch pathway and Forskolin and 3-isobutyl-1-methyl-xanthine (IBMX) for the Hippo pathway were used. Cells were treated for 8 hours as stated before in S1B. The values are reported as means of percentages of luciferase signal +/- SEM related to NΔE+DMSO (F) or DMSO (G) treated samples, indicated in the graph as "*ref*" (n=4). **(H)** Real-time PCR analysis of the transcription of β-catenin, Dickkopf (DKK1), Cyclin D1 and Axin1 in cells treated with 0.2% DMSO, 0.1% DMSO + 3 µM CHIR, 5 µM salinomycin + 3 µM CHIR, or 1 µM PAPTP + 3 µM CHIR. DMSO was used as negative control. All values were normalized on GAPDH expression. The values are reported as means of percentages of RNA expression +/- SEM related to DMSO + CHIR treated samples, indicated in the graph as "*ref*" for each gene (n=4). **(I-K)** GFP fluorescent Zebrafish Tg(12xGli.HSV:GFP)[ia11] Sonic Hedgehog (Shh) reporter fish (P), Tg(Olig2:GFP)[ek23] Oligodendrocyte reporter fish (Q), and dsRED fluorescent Tg(gata1:dsRed)[sd2] erythroid transcription factor Gata 1 reporter fish (R) were treated at 15 hpf for 15 hours with the following compounds: 3 µM CHIR; 10 µM cyclopamine (Cyclop), an inhibitor of the Shh pathway; 1 µM salinomycin (Salino); 1.5 µM PAPTP; 5 µM PCARBTP; 1 µM thapsigargin (Thapsi). DMSO 0.2 % was used as negative

control. Fluorescence quantification in the different animals, determined by GIMP 2.0 software, is shown. The lines represent the mean of the values +/- SEM related to DMSO treated samples, indicated as "*ref*" in the graphs. The number reported on the graphs represent the number of zebrafish embryos treated for each condition. For all the panels statistical significance (ANOVA) was determined (* = p<0.05; **=p<0.01; ***=p<0.001).
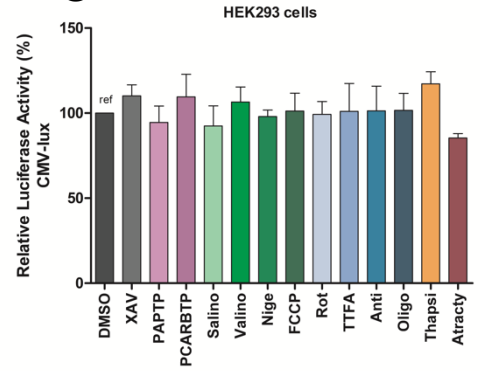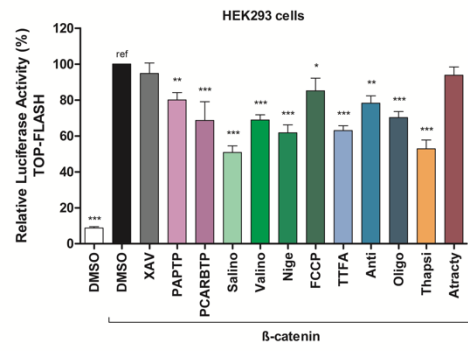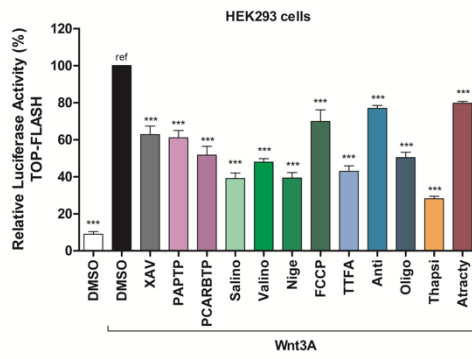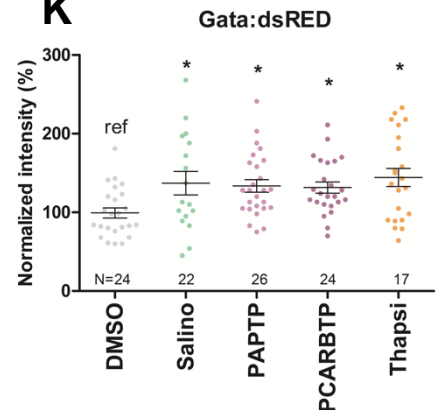
Suppl. Figure 1
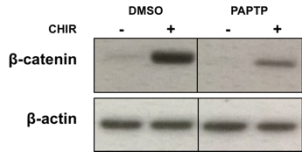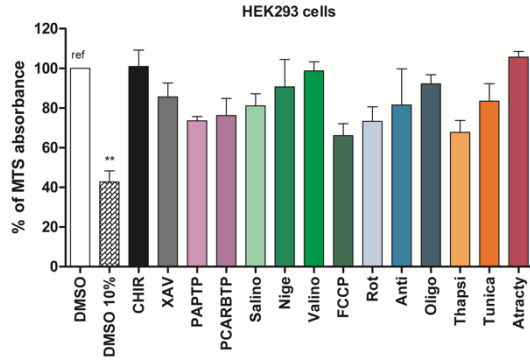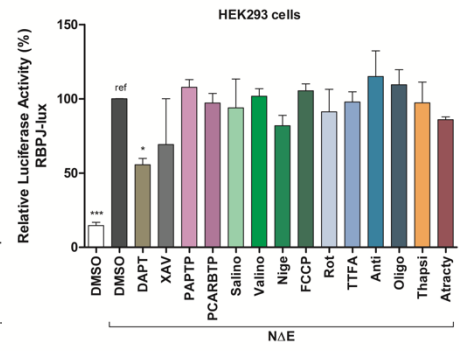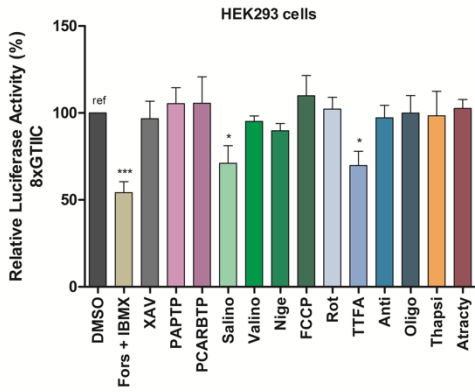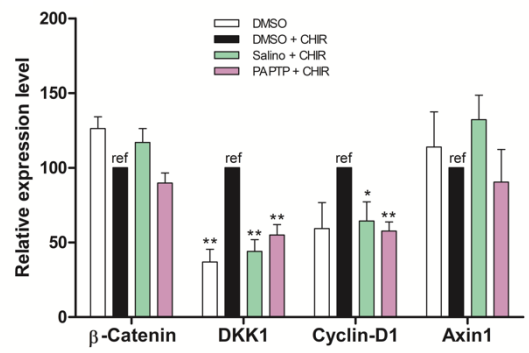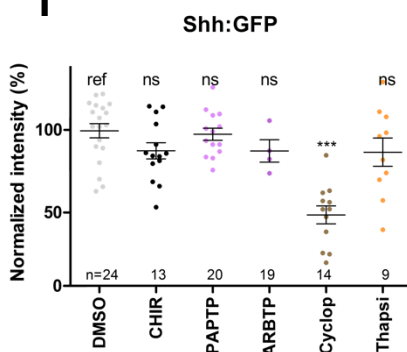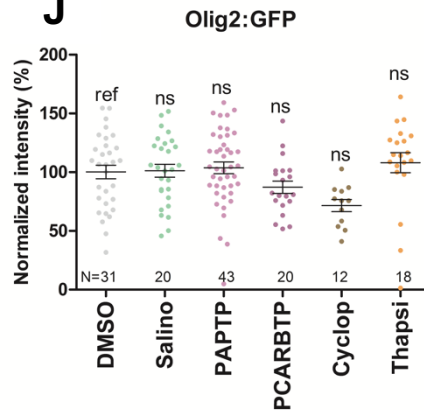
Figure S2. Other signaling pathways and non-canonical Wnt signaling are not activated by mito-Wnt axis. Related to Figure 2. (A) β-catenin phosphorylation in the serine 552 was observed by Western blot using 50 μg of total proteins extract from HEK293 cells treated as in S1B. A representative blot for the phosphorylated β-catenin protein is shown in the left panel, while the quantification of four independent experiments is reported on the right. β-actin was used as loading control. Values in the quantification are means of percentages +/- SEM related to the DMSO + CHIR treated sample, indicated as "*ref*". **(B)** AMPK activation was determined using the ACC phosphorylation on its serine 79 as readout. 50 μg of total protein extract from HEK293 cells treated as in S1B were analyzed by SDS-PAGE and then Western blot using a pS79 ACC antibody. Oligo was used as positive control, β-actin as loading control. A representative blot for the phosphorylated ACC protein antibody is shown on the left panel, while the quantification of three independent experiments is reported on the right. **(C)** Non-canonical Wnt signaling was measured by evaluating the expression of the Wnt5 ligand or the transcription factor NFATC1. Their expression was evaluated by Western Blot using 50 μg of total protein extracts from HEK293 cells treated as in S1B. β-actin was used as loading control. Representative blots for the Wnt5 or NFATC1 antibodies are shown in the upper panel, while the quantification of three independent experiments are reported below. **(D)** ER Ca^{2+} levels in HEK293 cells after 6 hours of treatment with the indicated compounds used as in figure 1A or 2A. Representative traces of the ER calcium reuptake are shown in the left panel, while the quantification at steady state is reported on the right (n=3; mean +/- SEM). The values are reported as Ca^{2+} concentrations, and analysis is related to the DMSO or 2-DG sample. **(E-G)** Effects of MFN2 WT overexpression on ER-mitochondria contacts. (E) Representative Western blotting analysis of MFN2, SERCA, Calnexin and Calreticulin overexpression in Hela cells wt or overexpressing MFN2. A representative blot is shown on the left panel, while the quantification of three independent experiments is reported on the right; (F) Representative confocal pictures of HeLa cells expressing $SPLICS_S$ alone (upper panel) or along with MFN2 WT (bottom panel). The green channel is the merge of several planes and refers to the signal emitted at 488 nm upon SPLICSs reconstitution. Scale bar 20 μm. Quantification of ER-mitochondria short contacts by 3D rendering of complete z-stacks is shown in the graph on the right (Ctrl, 60.7±5.3, n=40, 85.0 ±7.6 n=29, p<0.01). (G) ER Ca^{2+} measurement with ER-targeted low affinity aequorin. Upon ER Ca^{2+} depletion (see Material and Methods for details), the cells were perfused with KRB buffer containing 1mM $CaCl_2$ and the ER refilling was monitored. As shown in the Figure, after about 2 min a plateau is reached and it is indicative of the steady state Ca^{2+} concentration level in the ER lumen. The traces are representative of three independent experiments ($[Ca_{2+}]_{ER}$ mM, 168 ± 16.7 n=4 for CTRL and 227 ± 15.0 n=10 for MFN2 overexpressing cells p<0.05). **(H)** ER stress induction in HEK293 cells after the treatment as in S1B was further demonstrated by the induction of BiP shown by Western blot using 50 μg of total proteins extract per lane. A representative blot for the anti BiP antibody is shown on the left, while the quantification of three independent experiments is reported on the right. β-actin was used as loading control.
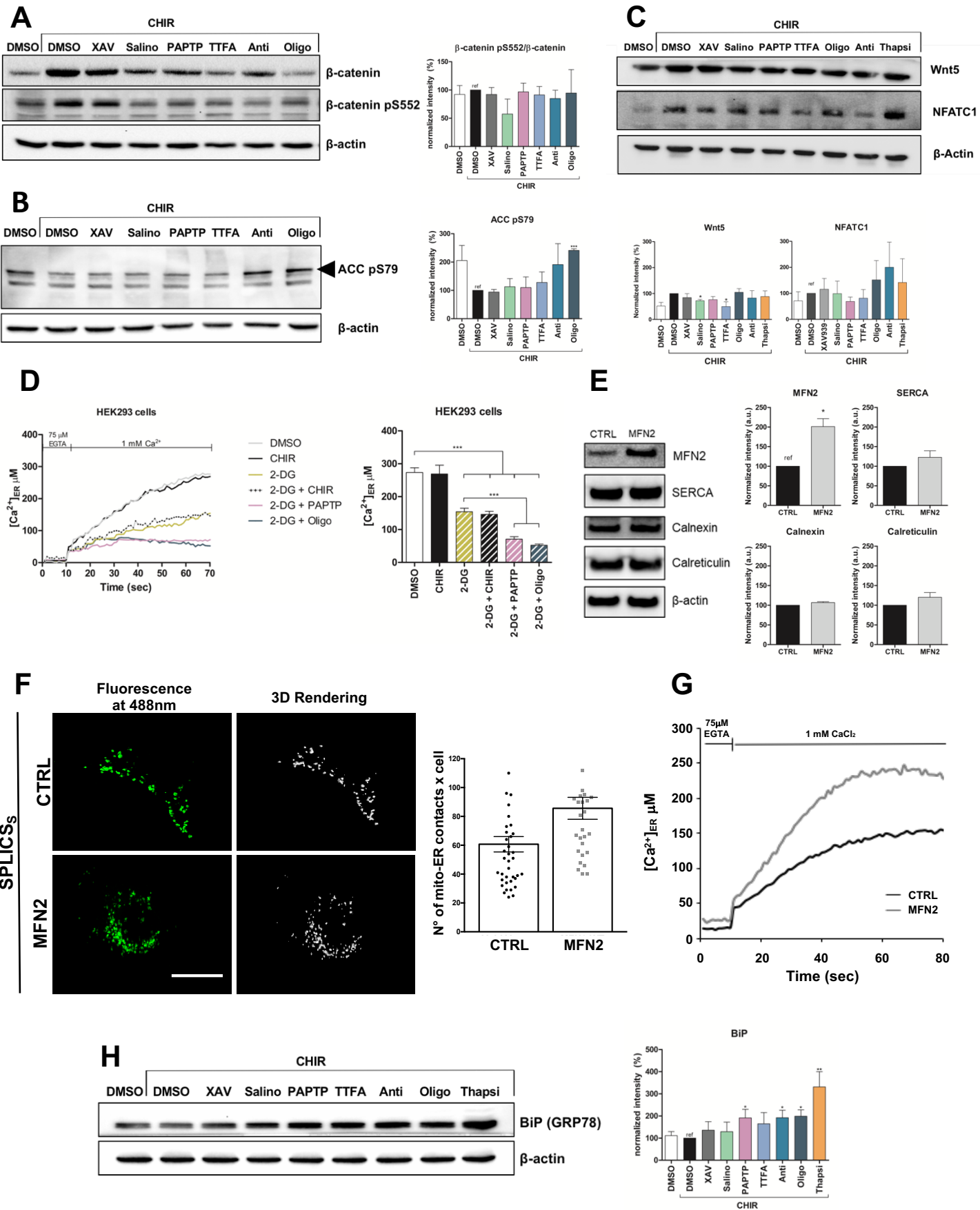
Suppl. Figure 2

Figure S3. Other signaling pathways and non-canonical Wnt signaling are not activated by mito-Wnt axis. Related to Figure 2. (A-B) Total Akt, Akt phosphorylation in serine 473, total GSK3β and GSK3β phosphorylation in serine 9 protein expression were evaluated by Western Blot using 50 μg of total proteins extract from HEK293 cells treated as in S1B after Wnt induction by Wnt3A plasmid transfection. β-actin was used as loading control. Representative blots are shown in A, while the quantification of three independent experiments is reported in B. **(C)** The ratio between the phosphorylated Akt (Akt pS473) or GSK3β (GSK3β pS9), as obtained in E, and the total Akt or GSK3β was quantified. Values in the quantification are means of percentages +/- SEM related to the DMSO+Wnt3A treated samples, indicated as "*ref*". For all the panels statistical significance (ANOVA) was determined (*=p<0.05; **=p<0.01; ***=p<0.001).
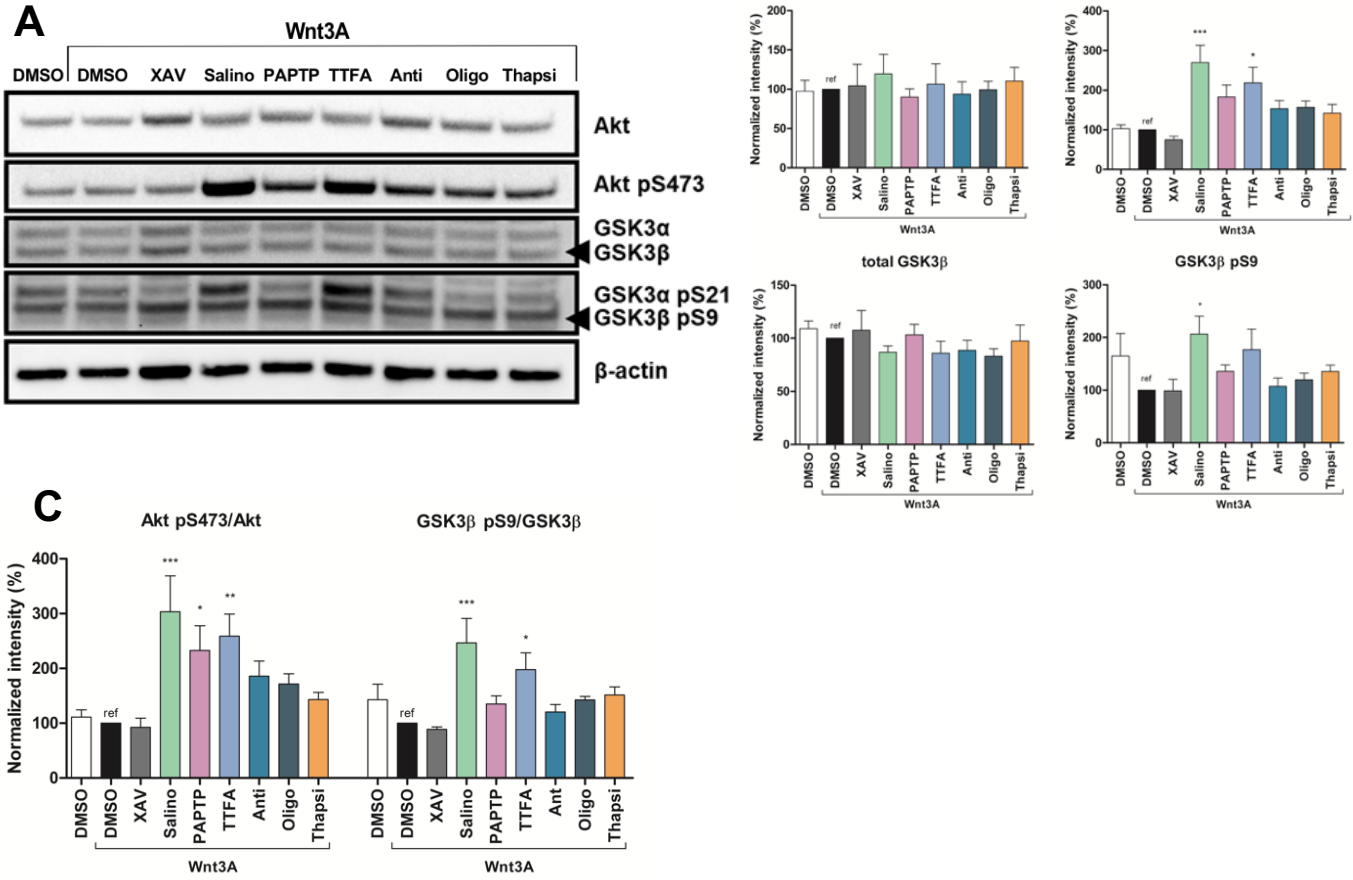
Suppl. Figure 3

Figure S4. Wnt signaling is down-regulated in colorectal cancer cells. Related to Figure 2. (A) Mitochondrial ATP content was measured in HCT116 cells after treatment with the indicated compounds at the concentration used in figure 2G. Cells were treated in a fresh medium containing 5 mM 2-deoxyglucose (2-DG) instead of glucose, in order to block glycolysis. The values are reported as percentage of luciferase signal related to the DMSO sample, used as negative control, and specified in the graph as "*ref*". Values are means +/- SEM (n=4). Oligo was used as positive control. **(B)** Viability of HCT116 cells was assayed after 24 hours of treatment with MTS assays, to confirm sub-lethal dosage of the compounds after the 8 hours-treatment used throughout the study. Cells were treated as in 2G. DMSO 10% was used as positive control. To better evaluate the effect of Anti, HCT116 cells were treated for 8 hours and then Annexin-V staining was performed to confirm that cell viability was not affected (data not shown). The values are reported as means of percentages +/- SEM of MTS absorbance measured at 490 nm related to DMSO-treated samples, indicated in the graph as "*ref*" (n=3). **(C)** Quantification of protein expression in HCT116 cells analyzed by Western Blot as reported in figure 2I. Values in the quantification from four independent experiments are means of percentages +/- SEM related to the DMSO treated samples, indicated as "*ref*". **(D)** Viability of DLD1 cells was assayed after 24 hours of treatment with MTS assays, to confirm sub-lethal dosage of the compounds after the 8 hours-treatment used throughout the study. Cells were treated as in 2G. DMSO 10% was used as positive control. The values are reported as means of percentages +/- SEM of MTS absorbance measured at 490 nm related to DMSO-treated samples, indicated in the graph as "*ref*" (n=4). **(E)** Canonical Wnt signaling activity based on TCF/LEF dependent transcription was assayed in DLD1 cells as in 2G for 8 hours. Analysis was performed as in 2G. Values are means +/- SEM (n=8). **(F)** Mitochondrial ATP content was measured in DLD1 cells after treatment with the indicated compounds at the concentration used in figure S2K. Cells were treated in a fresh medium containing 5 mM 2-deoxyglucose (2-DG) instead of glucose, in order to block glycolysis. The values are reported as percentage of luciferase signal related to the DMSO sample, used as negative control, and specified in the graph as "*ref*". Values are means +/- SEM (n=3). Oligo was used as positive control. **(G)** β-catenin and MET reduction and ER-stress induction were measured in DLD-1 cells (50 μg of protein extract/lane) by Western blot after treatment with the compounds as in S2K. β-actin was used as loading control. Quantification is reported on the right (n=4). Values in the quantification are means of percentages +/- SEM related to the DMSO treated sample, indicated as "*ref*". For all the panels statistical significance (ANOVA) was determined (*=p<0.05; **=p<0.01; ***=p<0.001).

Suppl. Figure 4